Combined inhibition of homologous immunotherapeutic targets PTPN1 and PTPN2 is synergistic in enhancing CD8 T cell effector functions.

Luis-Alberto Perez-Quintero[1,2], Zuzet Martinez-Cordoba[1,2], Cedric Carli[3], Alexandre Poirier[1,5], Samaneh Kamyabiazar[1], Chu-Han Feng[1,4], Alain Pacis[1,9], Yevgen Zolotarov[1,2], Kelly-Anne Pike[6], Jean-Sebastien Delisle[3,7,8], Michel L. Tremblay[1,2].

[1]Rosalind and Morris Goodman Cancer Institute, McGill University, Montréal, Québec, Canada; [2]Department of Biochemistry, McGill University, Montréal, Québec, Canada; [3]Centre de recherche de l'Hôpital Maisonneuve-Rosemont, Hôpital Maisonneuve-Rosemont, Montréal, Québec, Canada; [4]Department of Microbiology and Immunology, McGill University, Montréal, Québec, Canada; [5]Division of Experimental Medicine, McGill University, Montréal, Québec, Canada; [6]Ventus Therapeutics, Montréal, Québec; [7]Division of Hematology-Oncology, Hôpital Maisonneuve-Rosemont, Montreal, Québec, Canada and [8]Department of Medicine, Université de Montréal, Montréal, Québec, Canada. [9]Canadian Centre for Computational Genomics, McGill University, Montréal, QC, Canada.

Running title: PTPN1 and PTPN2 synergy in CD8 T cell responses.

Correspondence: Dr. M. L. Tremblay, Ph.D., Department of Biochemistry, Microbiology and Immunology, Rosalind and Morris Goodman Cancer Institute, McGill University, 1160 Avenue des Pins, Montreal, Quebec, Canada H3A1A3. E-mail: michel.tremblay@mcgill.ca

Abstract

Activation of cytolytic responses is proven fundamental for the control of tumoral cells. Increased understanding of the modulatory pathways controlling CD8 T cells had led to the formulation of successful checkpoint inhibitor-based immunotherapies against cancer. However, superfluous mechanisms acting to prevent immunopathology can further restrict immune activation. PTPN1 and PTPN2 are two homologous tyrosine phosphatases halting alternative CD8 activating pathways such as the proinflammatory cytokines and the TCR conferring them exceptional immunotherapeutic potential. Herein we investigated to what extent their homology translates into functional redundancy in CD8 T cells, exploring the potential benefits or risks of inhibiting them synchronously. Our results demonstrated that hemizygous deletion of PTPN1 in a PTPN2 deficient background heightens the enhanced effector phenotype already observed in PTPN2 defective CD8 T cells. This effect was evident in their transcriptomic signature and was reproducible with small-molecule inhibitors simultaneously hindering both phosphatases.

Introduction

PTPN1 and PTPN2 are two highly homologous nonreceptor protein tyrosine phosphatases [1]. In recent cent years, studies by us and others have underscored the potential of these phosphatases as immunotherapeutic targets [2-6]. Given the essential role of JAK and STAT proteins on the transduction of cytokine signals [1], these phosphatases, more specifically TCPTP had received much attention in their immunological roles. In fact, clues for an immunoregulatory role for TCPTP date back to the studies that generated its germline mouse deletion, this was the first genetic knockout mouse line generated for any PTP. It induced a severe phenotype characterized by immune dysregulation causing premature death [7, 8]. [7]. Homozygous mutants are viable after birth but die three to four weeks of age after with strong inflammatory signs detected by mononuclear infiltration in non-lymphoid organs and the presence of high levels of pro-inflammatory factors as IFN-γ, TNF-α and iNOS. The source of these cytokines is remarkably of non-hematopoietic origin, being mapped to the stromal cells in the bone marrow [9]. Further studies in these mice also showed a biased hematopoiesis that limited red blood cell formation and B cell maturation [10].

In contrast, mice deficient in PTPN1 were generally healthy and reproduced at mendelian ratios [11], yet showed minor immune system phenotype characterized by the accumulation of B cells in bone marrow and lymph nodes, an alteration that occurred downstream of common lymphoid progenitors [12]. Further hematopoietic dysregulation [13, 14] and altered immune reactivity were detected in PTPN1 KO mice after specific cytokine challenges [15]. Nonetheless, simultaneous germline deletion highlighted potential overlapping roles, particularly in the dephosphorylation of STAT1 [16]. Embryonic lethality of PTPN1 and PTPN2 double deletion in mice, strongly support

overlapping roles since single mutant animals for any of both enzymes, reaches birth at mendelian rates [9, 17].

CD8 T cells are essential immune system components in mounting antitumoral responses [18]. There is a positive correlation between the presence of CD8+ tumor infiltrating lymphocytes (TILs) and successful clinical outcomes in several types of cancer [19-21]. Moreover, cancer regression is observed after clonal CD8+ cell repopulation in melanoma patients[22], setting the grounds for exploring CD8+ cell based therapies. Indeed, redirection and/or reactivation of immune responses against cancer has been a remarkable source for novel therapies as immune checkpoint blockade [23, 24]. Immune checkpoint inhibitors (ICI), as anti-PD-1 directed antibodies, are extensively used for clinical trial and has been approved by the FDA for almost half of malignancies, nevertheless it still has a low estimated level of responsiveness of 12.5% and has failed to increase life span or progression free survival significantly [25]. Checkpoint inhibitors work by preventing/reversing a dysfunctional state of CD8 T cells known as exhaustion [26, 27]. Exhausted CD8 T cells are the result of chronic activation and is characterized by the expression of several inhibitory receptors including CTLA-4, PD-1, Tim-3, TIGIT, SLAMF6[28]. The limited success of ICI justifies the multifactorial nature of CD8 T cell dysfunction and encourage the search for novel strategies to prevent it. Indeed most of known checkpoint receptors act by modulating tyrosine phosphorylation through the recruitment of SHP-1 and SHP-2 phosphatases [28], hence the role of other regulatory phosphatases needs to be explored.

Herein, we analyzed CD8+ cells from mice with conditionally targeted deletions of PTPN2 and PTPN1 in mature CD8+ T cells. Whereas we found an enhanced functional state in PTPN2 single deficient cells, additional hemi-deficiency of PTPN1 greatly enhanced their pro-cytotoxic abilities, a phenotype that was mimicked using small molecule inhibitors targeting both phosphatases.

Results.

Combined deletion of PTPN1 and PTPN2 alters CD8 T cell differentiation

To address the combined contribution of PTPN2 and PTPN1 to the regulation of activating signals in CD8+ T cells we designed a mouse line where allelic inactivation of either one or both genes occurs in mature, post-thymic CD8 T cells. To achieve this, we breed heterozygous mice carrying "floxed" alleles of both genes, PTPN2 [29] and PTPN1 [30], with a mouse line where the CRE recombinase expression is driven by the CD8 enhancer 8I (E8i-CRE) [31]. Mice were bred to produce littermates with either WT (wt/wt), heterozygous (wt/fl) or homozygous (fl/fl) versions of either single or both genes (Figure S1A). To avoid potential artifacts arising from off-target effects of the CRE recombinase [32, 33], mice heterozygous for E8i-CRE (wt/cre+) carrying wt alleles for PTPN2 and PTPN1 were used as controls, hereafter named CRE. Mice were born at mendelian rates, and no apparent differences were detected between the various genotypes until 6-8 weeks of age. CD8 T cells from all genotypes reached maturity and were distributed in peripheral secondary immune organs (Figure 1). To confirm that conditional deletion of both genes was achieved, we tested the protein expression of PTPN2 and PTPN1 by immunoblotting in both, peripheral CD4 and CD8 T cells (Figure S1B). As expected, protein expression corresponded to each genotype, and deletion was not observed in CD4 T cells. Nevertheless, mice around 8-10 weeks of age in which CD8+ T cells lacked expression of both genes (ptpn1 fl/fl; ptpn2 fl/fl; wt/cre+) or dKO hereafter, showed a significant reduction in thymus size with complete involution observed around 12 weeks of age (Figure S1C). Microscopically, cortical and medullary architecture was lost in the thymi of these mice when compared to CRE controls (Figure S1D). In the same mice, we observed mild splenomegaly and spontaneous lymphadenopathies (Figure

S1E). In contrast to dKO mice, other genotypes did not show differences in organ size or cellularity when compared to CRE controls.

Next, we characterized circulating CD8 populations from the different genotypes by flow cytometric analysis. Although CD8 T cells were present in the spleen and lymph nodes of all the genotypes analyzed, mice with dKO CD8 T cells showed an increase in the CD4/CD8 cell ratio in lymph nodes, however, the absolute number was not significantly affected (Figures 1A, 1B and S1F). This finding, together with the size increase of lymph nodes suggested a change in the migratory cues of lymph nodes. No other significant differences in the distribution of T cells in lymph nodes or spleen were noted. However, we detected a subpopulation of splenic CD8 T cells expressing low levels of the CD8 coreceptor in both, dKO and N2KO/N1Het (Ptpn1 wt/fl; Ptpn2 fl/fl; wt/cre+) mice (Figures 1A and 1D). Accumulation of these CD8low-expressing cells was more pronounced in the dKO animals, almost doubling those seen in the N2KO/N1Het animals, comprising around 70% and 40% of all splenic CD8 T cells, respectively (Figures 1C and 1D). Cells displaying this phenotype were also observed in CRE controls, and both single KO. Yet they were present at a much lesser percentage (ranging from an average of 13% to 17%) and differences were not statistically significant (Figures 1C and 1D). To further characterize peripheral CD8 T cells in these animals, we assessed their differentiation state by co-staining for the trafficking molecule CD62L and the memory marker CD44 (Figure 1E). We sorted different CD8 T cell subpopulations of the spleen and peripheral lymph nodes based on L-selectin (CD62L) and CD44 surface molecule expression defining naïve, effector/effector memory, and central memory subpopulations (Figure 1E and 1F). While the differentiation state of CD8 T cells in lymph nodes seemed unaffected within the various genotypes, spleens showed a marked increase of effector/effector memory-like CD8 T cells in the N2KO/N1Het mice (Ptpn1 wt/fl; Ptpn2 fl/fl;

wt/cre+) and dKO mice. This subset of CD8+ T cells, characterized by reduced expression of CD62L and intermediate expression of CD44, correlated with the presence of CD8low cells (Figure 1D). To determine if this correlation was indeed given by a distinct differentiation state of the CD8low subpopulation, we next compared the expression of know CD8 differentiation markers in these cells with the CD8high subpopulation. Besides CD44 and CD62L, we evaluated the expression of the transcription factor EOMES, the IL-7 receptor CD127, and the terminal differentiation marker KLRG1 (Figures 1G and 1H). In general, we found that CD8low cells from the N2KO/N1Het and dKO mice, besides a strong effector phenotype given by low CD62L and increased CD44 expression, showed a terminal effector phenotype characterized by loss of CD127, a slight increase in KLRG1 but low levels of the transcription factor EOMES. These surface phenotypical characteristics define this subpopulation as short-lived effector CD8 cells [34]. Hence, in these two genotypes, CD8+ T cells tended to spontaneously differentiate into terminal effector cells with preferential migration to the spleen.

PTPN1 deficiency potentiates pre-existent functional enhancement in PTPN2 KO CD8 T cells

To understand the functional capabilities of the CD8 T cells with combined deficiency of PTPN2 and PTPN1, we breed our colony of conditional mutant mice with OT-1 transgenic mice. OT-1 mice express a TCR with affinity for an epitope of chicken ovalbumin (OVA 257-64), recognized in the context of the MHC Class I haplotype H2-Kb expressed on C57BL/6 mice [35]. We generated in vitro OVA-specific activated cytotoxic lymphocytes (CTL) from purified naïve splenic CD8+ T cells. The use of Naïve CD8 T cells allowed us to start from homogeneous populations and prevent artifacts originating from the use of different ratios of naïve, effector, and memory cells observed in the different genotypes in Figure 1. After 4 days of expansion by

stimulating them with crosslinking antibodies for CD3 and CD28, and recombinant murine IL-2, OT-1 naïve CD8 T cells give rise to a mixed population of in vitro cytotoxic lymphocytes (CTL), which conserved expression of the transgenic TCR α and β chains, hence maintaining specificity for the OVA epitope. The expression of these chains was equivalent to that observed in CTL generated by stimulation with the cognate peptide SIINFEKL and antigen-presenting cells (APCs) (Figure S2A). Day 4 CTL cells from naïve CD8 T cells (used from here on, otherwise specified) were then challenged with the OVA expressing thymoma cell line E.G7 in 5-hour in vitro cytotoxicity assays (Figures 2A, 2B, and S2B). In our hands, regarding the single mutant cells, we observed an increase in the cytolytic activity of CTL deficient for PTPN2 when compared to CRE controls, however, CTL from mice lacking PTPN1 showed no significant increase. The enhanced effector activity seen in the PTPN2 deficient cells is in line with previous observations by Sharpe's and Tiganis' groups [4, 5]. Remarkably, we consistently observed a significant increase in the cytolytic activity of CTL from N2KO/N1Het and dKO genotypes over those with sole PTPN2 deficiency. This increase was evident at different effector-to-target ratios, being almost twice the fold at 5:1 and 10: ratios when compared to the single N2KO cells (Figures 2A, 2B, and S2B). Secretion of proinflammatory cytokines, such as IFN-γ, is also a characteristic of effector CD8 T cells. Consequently, we measure the presence of this cytokine in the supernatant by ELISA. We detected an increase in the secretion of IFN-γ in PTPN2 and PTPN1 single deficient cells at low effector-to-target ratios which were more stepped in the PTPN2 KO cells (Figure 2C). However, a significant reduction of IFN-γ concentration was observed in the supernatants from dKO CTLs, which was more evident in low effector-to-target ratios. No substantial changes were seen in the N2KO/N1Het, which were conversely the most efficient at tumor lysis (Figure 2C). As CD8 differentiation dictates the functional state of these cells, we sought to analyze by flow cytometry

the expression of the CD62L and CD44 surface markers on these in vitro-stimulated CTLs (Figures 2D and 2E). We observed a clear deviation in all the genotypes towards the effector/effector-memory population compared to the CRE controls, including the single N1KO cells. While this shift towards an effector phenotype could explain the increased cytotoxic activity of CTL from deficient cells, we did not find a direct correlation between these two readouts, suggesting other mechanisms rather than differentiation participate in the functional enhancement observed (Figure S2C).

Dual specific PTPN1/PTPN2 inhibitor recapitulates genetic deficiency

The effect that we observed on CD8 T cell activity after combined inhibition of PTPN1 and PTPN2 has the potential to reverse inhibitory cues in immunosuppressive microenvironments, such as tumors. With this in mind, we aimed to test small molecule inhibitors targeting specifically PTPN2 and PTPN1, taking advantage of their similarities in their catalytic domain [36, 37]. L598 is a competitive orthosteric soluble compound that can inhibit both phosphatases with equivalent IC50 [38]. As the main known substrates of PTPN2 and PTPN1 are transcription factors or signaling components lying close upstream, we assumed that the functional changes observed in genetic deficiency required modulation of gene expression. Hence, we activated splenic naïve CD8 T cells from OT-1mice to generate CTL *in vitro* in presence of various concentrations (2, 5, and 10 µM) of L598 that were maintained during the differentiation/expansion process. We tested these CTL on day 4 in cytotoxic assays against E.G7 targets (Figures 3A and 3B). Treatment with the compound significantly increased the cytotoxic activity of CTL against targets at all concentrations (Figure 3A and 3B) reaching its highest at 5µM. Nevertheless, we did not observe significant differences between 5µM and 10µM, uncovering a plateau concentration for the effects of the inhibitor. The enhancement of cytotoxicity seen in L598 treated cells was independent of the

method used to produce the ex vivo CTL, as we were able to detect a similar increase in the activity when these cells were generated by stimulation with the cognate peptide and APCs (Figure S3A). As cytokine secretion seems to be also affected by the reduced activity of PTPN2 and PTPN1, we quantified IFN-γ secretion in the supernatant of these experiments by ELISA (Figure 3C). As observed in genetically deficient cells, IFN-γ secretion was higher in the lower effector-to-target ratios, suggesting that low levels of stimulation favor proinflammatory cytokine secretion. Alongside, the presence of the inhibitor at a low concentration (2μM) correlated with a more significant increase in the secretion of IFN-γ, resembling observations in the single PTPN2 or PTPN1 deficient cells. Additionally, increasing the concentration of the inhibitor led to an opposite effect in IFN-γ secretion, like that observed in the N2KO/N1Het or the dKO-derived CTLs.

Next, we evaluated by flow cytometric analysis how the differentiation state of CD8 T cells was altered by the treatment with L598 (Figures 3D and 3E). Despite the functional enhancement observed with 5 and 10 μM, the expression of CD62L and CD44 drifted towards a gradual increase of the Tcm population (CD62L high, CD44 high events; Q2) and correlated with the inhibitor concentration used (Figure 3E). Hence, treatment with L598 either potentiate the function of effector differentiated cells or confers effector characteristics to cells phenotypically characterized as Tcm. Moreover, when we generated CTL through the stimulation of naïve CD8 T cells with the cognate peptide, differentiation modestly drifted towards an increase in the proportion of effector/Effector memory cells when cells were in the presence of L598 (Figure S3B). In contrast, their cytotoxicity capacity was increased at least twice that observed in untreated cells (Figure S3A). To test if the functional phenotype seen after treatment with L598 is indeed a consequence of specific inhibition of PTPN2 and PTPN1, we treated CD8 T cells with different genotypes used previously with 5μM L598 during invitro CTL differentiation. We tested for specific cytotoxicity

against E.G7 cells (Figure 3F). As seen in WT OT-1 CTLs, CRE controls increased their capacity to lyse target cells by about twice a fold. In the case of PTPN1 single deficient cells, cytotoxicity followed a pattern without significant differences to CRE controls either when treated or not with the inhibitor. Remarkably, PTPN1 deficient CTLs treated with the inhibitor increased their cytolytic capacity to that of PTPN2 single deficient cells. These results suggest a primary requirement of PTPN2 inhibition for the enhanced activity observed in CD8 cells, and the ability of the inhibitor to target PTPN2 activity intracellularly. However, after treatment with the inhibitor, PTPN2 single deficient cells still increased their cytolytic activity twice more than when compared to non-treated cells. This increase resembled at the same time the increase observed when comparing the PTPN2 KO with N2KO/N1Het CTLs. Hence, PTPN1 is targeted intracellularly by the inhibitor and the pharmacological inhibition with 5µM L598 had a comparable effect to the observations in the PTPN1 hemizygous cells. Remarkably, the inhibitor did not influence either N2KO/N1Het or dKO CTLs cytotoxic capacities suggesting that, in both genotypes, cells are brought to their maximum effector capabilities (Figure 3F). Following this, we measured IFN-γ in the cell supernatant of these experiments. As observed previously, cells stimulated at a 5 to 1 effector to target ratio in either genetically deficient in PTPN2 or those treated with the inhibitor had the highest IFN-γ secretion (Figure 3G). In general, as seen in the previous experiments, reduced activity of PTPN2 and PTPN1 led to a decrease in the secretion of IFN-γ.

Ex-vivo treatment of human T cells with L598 enhances proinflammatory cytokine secretion and Tcm differentiation

We tested, as well, the capacity of L598 to ameliorate the functionality of human T cells. To do so, we enriched T cells from healthy donors' PBMCs and stimulated them in vitro with anti-CD3 and anti-CD28 for 7 days in the presence of increasing amounts of L598. On day 7 cells were

harvested and analyzed by surface and intracellular flow cytometry for the pro-inflammatory cytokines IFN-γ and TNF-α, as for the differentiation markers CD45RO and CD62L defining effector and memory populations. In vitro treatment of human T cells with L598 led to an increase in the production and accumulation of both IFN-γ and TNF-α in both CD4 and CD8 T cells (Figure 4A, 4B, S4A, and S4B). In all cases, the increase reached its maximum with 2μM treatment and was maintained at a similar extent when cells were treated with increasing concentrations. The increase in cytokine production was around 30 to 40% for TNF-α and 50 to 70% for IFN-γ, in both CD4 and CD8 T cells. Besides increased proinflammatory cytokine production, we also observed that treatment with L598 skewed T cell differentiation towards a central memory phenotype (CD45RO high, CD62L high) in both CD4 and CD8 T cells (Figure 4D). This increase was more pronounced in CD8 T cells and seemed to correlate to the concentration of L598 used. We did not find any preference for improving CD4 or CD8 T cell proliferation as both cell types were similarly represented at the different concentrations used of L598 (Figure S4C).

Signaling through the Jak/STAT pathway is largely dysregulated in PTPN1 and PTPN2 deficient cells

Type I interferons have a critical role in CD8 T cell acquisition of effector and memory functions [39, 40] and signal strongly through STAT1 [41], one of the main targets of PTPN1 and PTPN2 regulation. To investigate how the combined absence of these phosphatases modifies type I interferon signals, we stimulated CTL carrying different genotypes with IFN-β for 10 and 30 minutes. We analyzed phosphorylation levels on the canonical dimerizing c-terminal phospho-tyrosine residues by immunoblotting with specific antibodies. In our experiments, CRE control cells responded to recombinant murine IFN-β by increasing phosphorylation of these residues in STATs 1, 2, 3, 4, and 5a (Figures 5A and 5B) revealing the complexity of type I interferon signals

in CD8 cells. No increase in the phosphorylation of STAT6 was observed either in CRE control cells or in any of the genotypes analyzed (Figure 5B). The deficiency of either of these phosphatases resulted in the increased phosphorylation of STATS 1, 3, and 5, while phosphorylation levels of STAT4 seemed unaffected. A similar responsive pattern was observed in cells from N2KO/N1Het confirming that these cells are more sensitive to stimulation with type I interferons. Conversely, dKO cells were highly hyporesponsive with decreased phosphorylation of STATS 1, 3, and 5. Although the ratio of phosphorylated STAT4 to total protein was conserved, a clear restriction in protein expression in these cells resulted in the low availability of the phosphorylated version. Unstimulated dKO cells were largely different from unstimulated controls as well, showing STAT protein expression and levels of phosphorylation affected. Notably, and in opposition to STAT4, we detected increased expression of STATs 1 and 3, accompanied by increased basal level phosphorylation of STAT3. Higher expression and basal phosphorylation of STAT3 also gradually appear in N2KO and N2KO/N1Het samples, an aspect of the dysregulation induced by PTPN1 and PTPN2 deficiency that followed a pattern like that of the increase in cytotoxicity, hence potentially related directly to the global changes in transcription occurring in these cells.

Transcriptional changes induced by PTPN1/PTPN2 deficiency emulate pre-exhausted effector CD8 T cells

Combined deficiency of PTPN1 and PTPN2 resulted in a synergistic enhancement of effector functions in CD8 T cells, this was accompanied by several changes in the expression and activation of STAT transcription factors, either at baseline or after cytokine stimulation as IFN-β. To understand the extent of the transcriptional changes promoted by the deficiency of PTPN1 and PTPN2, we performed bulk mRNA sequencing of day 4 CTL derived from the different genotypes

and cells treated with L598. We aimed to identify the differentially regulated transcripts by comparative RNAseq (Figures 6 and S4). Unsupervised principal component analysis (PCA) revealed that the samples acquired a progressive drift from controls which correlated with the reduction of PTPN1 expression on the PTPN2 deficient background (Figure 6A). Conversely, cells with intact expression of PTPN2 but deficient in PTPN1 diverged from other genotypes analyzed and mapped the farthest to CRE controls (Figure 6A and C), strongly suggesting that both phosphatases target, at least partially, non-redundant pathways. The progressive drift observed in the PCA was also reflected in the number of significant differentially expressed (DE) genes (Figure S5A). As our interest was centered on the genes involved in the enhancement of the effector functions of CD8 T cells as a result of the reduction of PTPN1 activity in a PTPN2 deficient background, we targeted the differentially expressed genes between the PTPN2 KO cells and the PTPN1 Het/PTPN2 KO (Figure 6B and Table S1), as the later genotype showed similar levels of increase in their specific cytotoxicity than the dKO but allowing us to study the differences in an environment with less transcriptional drift, providing a more restricted set of hits. Following this, we identified 376 DE genes (Table S1 summarizes DE genes for which the log2 fold change was greater or lower than 0.5); in this list we found a transcriptome leaning towards an effector phenotype, characterized by positively regulated effector genes as Prf1, Gzmb potentially as a consequence of downregulation of the transcription factors Tcf7 and EOMES [42], and downregulation of the naïve/memory marker Sell (CD62L). We also noticed the triggering of counter-modulatory mechanisms as the inhibitory receptor klrk1, the Jak/STAT regulator ASB2 and the cytokines IL-10, Tgfb3, and cytokine receptor for IL-13, IL-13ra1, potentially upregulated by the presence of the transcription factor Maf which transcript was found also increased. A heat map analysis highlighted that, although most of the differential genes observed in this comparison

are a reinforcement of the N2KO transcriptional footprint and opposite to the N1KO, a few areas coincided in expression to the N1KO (Figure S5B). We also analyzed a comparative transcriptional signature between Day 4 CTL from C57BL/6 naïve spleen CD8 T cells treated or not with 5µM L598. When added to the PCA plot, these cells drifted partially towards the dKO cells but opposite to the N1KO cells (Figure S5C), suggesting that the inhibitor-induced partial inhibition of both enzymes at the used concentration.

Given the large amount of data generated, we used a biased approach to emphasize the transcriptomic signature of the different groups analyzed based on genes with known relevancy in CD8 T cell biology. (Figure 5C). As our previous data suggested, PTPN2 deficiency corresponded to an increase of effector molecule expression as granzymes and perforin, reduction of migratory receptors to secondary immune organs, such as CD62L and CCR7, mild expression of inhibitory receptors such as PD1, Tigit and Tim-3, and increase of chemokines CCL3, 4 and 5. Remarkably, the deletion of PTPN1 potentiated this effector phenotype in the PTPN2 deficient background, an effect that correlated to the number of alleles deleted, been more evident in the dKO than in the N2KO/N1Het cells. Correspondingly, the transcriptome of CD8 T cells treated with L598 highly resembled that of the N2KO and N2KO/N1Het confirming that the mechanisms improving the effector qualities of cells treated with L598 are given by similar changes observed in the deficient genetic cells. In contrast, there was a large discrepancy in the transcriptomic signature of the PTPN1 deficient cells compared to all others analyzed. N1KO cells transcriptome resembled memory cells, characterized by the upregulation of the IL-7 receptor CD127, CD62L, CXCR5, and CD28, and upregulation of the transcription factor Tcf1. These cells also showed characteristics of terminal effector T cells, like a high expression of the inhibitory receptors Tigit, SLAMF6, CD38, and CTLA4. Similarly, although the transcriptome of dKO cells correlated to

that of single PTPN2 KO cells, these cells also expressed higher levels of receptors associated with terminal differentiation, such as Tim-3, Tigit, Lag3, Entpd1, and PD-1. However, in the dKO genotype, we also observed ectopic expression of the Th17-related transcription factor Rorc suggesting that transcriptional dysregulation in these cells could result in aberrant differentiation transition to Th17-like phenotype, a phenomenon observed in CD4 Treg cells with PTPN2 loss of function mutations [43]. dKO cells also showed a marked deviation towards a dysfunctional state as we detected increased upregulation of the three members of the transcription factor family NR4A (Figure S5D) in dKO cells over all the other genotypes analyzed, which is associated with the establishment of exhaustion in CD8 T cells [44]. However, no upregulation of the exhaustion-related transcription factor Tox was observed (Figure 6C), indicating that chronic stimulation through pathways other than those controlled by PTPN1 and PTPN2 is required to establish exhaustion.

Dual inhibition of PTPN1 and PTPN2 induces the upregulation of several effector-related transcription factors

We scrutinized our mRNA analysis for transcription factors known to positively drive CD8 effector differentiation (Figure S6A). We confirmed by immunoblotting an elevation of protein products for BatF3, IRF4, Myb, ZEB2, and BLIMP1 (Figure 7), suggesting that transcriptomic changes observed between the different genotypes have indeed a multifactorial origin. Between those, BatF3 was the most significantly upregulated transcription factor with a known role in CD8 T cells that we observed in our analysis, and which correlated with the onset of the cytotoxic phenotype increase seen in the different genotypes analyzed. Henceforth, we considered the upregulation of BatF3 a potential downstream mechanism for the functional enhancement seen after PTPN2/PTPN1 inhibition. BatF3 is linked to the differentiation of CD8+ dendritic cells into

a phenotype with enhanced capacities to activate CD8+ T cells, named conventional DC type I (cDC1) [45]. Although no large pool of evidence has been reported for this TF in CD8+ T cells, it has been linked to the formation of CD T cell memory [46]. We sought then to evaluate a possible link of BatF3 with the enhanced CD8+ cytotoxicity. We "knocked down" the expression of this TF using siRNA during in-vitro differentiation of N2KO/N1Het CTLs under the OT-1 background. Using the EG.7 cytotoxicity assay as a readout, we compared the functional effector properties of N2KO/N1Het cells with reduced expression of BatF3 (Figure S6A). There were no appreciable differences in their cytotoxic ability against E.G7 cells when compared to controls transfected with a nontargeting siRNA oligo, despite a clear reduction of BatF3 expression (Figure S6B). Even so, BatF3 deletion did not affect functionally N2KO/N1Het cells, the regulation of transcription by PTPN2/PTPN1 could be multifactorial.

Discussion

Recent publications link either PTPN1 or PTPN2 inhibition with enhanced antitumoral responses [3, 5, 6, 47]. Even though they share high homology and previous publications outline evidence of partial redundancies [2, 16] their combined inhibition in CD8 T cell function has not been explored. Genetic deficiency of both genes resulted in unexpected functional gains revealing redundancy in their regulatory role in CD8 T cells. The extent of these gains correlated to the number of alleles deleted, with double-deleted mutant CD 8 T cells, dKO, showing the most extreme phenotype. In these mice, up to 80% of peripheral CD8 T cells in young immunologically unchallenged mice revealed a terminal effector/effector memory phenotype compared to a 10% observed in CRE controls or single mutants. Unexpectedly, around 8 to 10 weeks of age these animals revealed premature thymic involution, an organ failure not seen in any of the other genotypes studied. This extreme phenotype was also apparent at the transductional and

translational levels. Expression and phosphorylation of STAT proteins, a main target of PTPN1 and PTPN2, were largely divergent in dKO CD8 T cells compared to controls and other genotypes analyzed. Indeed, dKO CD8 T cells expressed significantly larger amounts of STAT1, lesser STAT4, and increased basal phosphorylation of STAT3. As well, these cells showed the largest number of significant differentially expressed genes, while mapped as the most transcriptionally distant to CRE controls of all the genotypes analyzed. Differentiation of dKO CD8 T cells was characterized by a high expression of inhibitory receptors such as Tim-3, TIGIT, LAG-3, CD244a, PD1, and Entpd1, characteristically seen in chronically stimulated cells [48]. In accordance, these cells expressed highly all the members of the NR4A family of transcription factors, known to be upregulated in CD8 exhausted cells [44]. However, dKO CD8 T cells were highly functional, as shown by their cytotoxic capacity, and they presented low expression of the transcriptional factor Tox [49-51]. Hence, their differentiation state resembles that of terminal effector cells, which lie upstream of the onset of exhaustion, and suggests that chronic stimulation through other pathways is required for reaching a dysfunctional state. Additionally, dKO CD8 T cells also showed ectopic upregulation of RorC, a transcription factor related to CD4 T cells differentiation into Th17 cells. Together with our previous findings on the effects on embryo development of germline deletion of both genes [16], these data support the idea that total deletion of both phosphatases induces strong developmental and differentiation dysregulation that can be prevented by partial expression of either one copy of PTPN1 or PTPN2. On this, the use of competitive inhibitors is extremely suited for partially inhibiting these enzymes, thus preventing the dysregulation noted in full dKO CD8 T cells.

Regarding the single deficiency of PTPN2 in CD8 T cells, we were able to confirm the findings by others as it confers better effector qualities against tumors, increasing cytotoxicity and IFN-γ

secretion while protecting them from exhaustion [4, 5]. Remarkably, we found that when PTPN2 deficiency is accompanied by partial deletion of PTPN1, N2KO/N1Het cells, the cytolytic capacity of these cells was equivalent to that of the dKO cells. Notwithstanding, N2KO/N1Het mice and CD8 T cells did not exhibit the extreme phenotypical or transcriptional changes observed in dKO cells and their cytotoxicity rested them in between the N2KO and the dKO phenotypes. Despite single PTPN1 deficient CD8 T cells being divergent from PTPN2 deficient cells, the transcriptomic signature of N2KO/N1Het accurately resembled that of the PTPN2 single deficient cells, an observation extended to double deficient cells. The gradual acquisition of the phenotype was reflected in the increased expression of several transcription factors associated with CD8 T cell differentiation, such as BatF3, IRF4, Myb, ZEB2, and BLIMP1. Basal phosphorylation of STAT3, previously associated with the phenotype seen in PTPN2 deficient T cells [52], followed a similar stepwise increase. Therefore, partial inhibition of PTPN1 in a PTPN2 null background proved of benefit to increase the cytolytic activity of CD8 T cells.

Although we saw a direct correlation between the cytotoxic capacity of CD8T cells to the degree of functional silencing of PTPN2 and PTPN1, secretion of IFN-γ did not follow such linearity. Instead, we observed a peak production with mild inhibition, dictated either by low or intermediate concentrations of L598 or by deleting each gene apart, but importantly, at higher levels of combined genetic/pharmacological inhibition, the production of IFN-γ decreased. We interpreted this discrepancy between readouts of effector function as the triggering of independent feedback mechanisms. We believe that a better understanding of this mechanism would broaden the range of molecular targets for future therapeutic intervention.

Finally, our data offer a mechanistic insight into the advantages of developing dual PTPN2/PTPN1-specific inhibitors in immunotherapeutic settings. The high homology between

both catalytic domains provides a foundation to prevent out-of-target consequences. Given its transductional independence from other T cell checkpoint pathways, combinatorial use of PTPN2/PTPN1 inhibitors with already approved ICI therapies is a foreseeable step. Furthermore, PTPN2/PTPN1 inhibition does not require to be T cells specific as effects in the tumoral [3] and other immune components, such as dendritic cells [2], promote further antitumoral activity.

Acknowledgments

This work was supported by a Canadian Institute of Health Research Foundation grant (CIHR FDN-159923), the Richard and Edith Strauss Canada Foundation, and the Aclon Foundation to MLT. MLT holds a Chair of the Jeanne and Jean-Louis Levesque Foundation in Cancer Research. LAPQ is the recipient of a Cole Foundation postdoctoral fellowship, ZMC received support from the Quebec provincial MITACS awards, and AP and CHF are recipients of the FRQS training studentships. We thank the "Comparative Medicine and Animal Resources Centre "(CMARC) at McGill University for their veterinarian and animal husbandry services. We are grateful to the Flow Cytometry and Bioinformatics cores at the Rosalind and Morris Goodman Cancer Institute for their help in technical aspects and experimental design.

Disclosure

As for conflict of interest, MLT is a co-founder of Kanyr pharma inc. and act as its scientific chief officer (SCO), MLT is also co-founder and board member of Mispro Biotech Services. No other authors declare conflicts of interest to disclose.

Data availability

Details for accessing the bulk mRNA sequencing data supporting the findings in this manuscript is available in BioProject repository under the accession number: PRJNA869093.

Materials and methods

Mice and cell lines

All mouse procedures were performed using 6-12 weeks old C57BL/6 mice according to the Canadian Council on Animal Care ethical regulations and were approved by the McGill University Research and Ethics Animal committee. For conditional deletion in CD8 T cells, mice expressing CRE under the E8i enhancer [31] were bred with mice carrying "floxed" versions of the ptpn1 [30] and ptpn2 alleles [29]. For specific cytotoxicity, mice were crossed with C57BL/6-Tg (TcraTcrb)1100Mjb/J "OT-1" animals purchased from The Jackson Laboratory. For tumor implantation, 6-8 weeks old C57BL/6J male mice were purchased directly from The Jackson Laboratory. Complete necropsies of CRE controls and dKO animals were performed by the Charles River Research Animal Diagnostic Services. E.G7 cell line, a derivative of the EL4 mouse thymoma cell line expressing chicken ovalbumin (OVA), was purchased from ATCC.

Antibodies and reagents

For flow cytometry, the following anti-mouse antibodies were acquired from Biolegend CD3 (145-2C11), CD4 (GK1.5), CD8 (53-6.7), TER119 (TER119), Ly-6G/Ly-6C (RB6-8C5), B220 (RA3-6B2), CD11b (M1/70) and KLRG1 (2F1/KLRG1). Antibodies against mouse CD62L (MEL-14) and CD127 (SB/199) were from BD Biosciences. Antibodies against CD44 (1M7) and EOMES (Dan11Mag) were from eBiosciences.

Anti-human antibodies were acquired from BD Biosciences for, CD3 (SK7), CD4 (RPA-T4), CD45RO (UCHL1), CD62L (DREG-56), IFN-γ (4S.B3), TNF-α (MAb11) and ThermoFisher Scientific for CD8 (RPA-T8).

For immunoblotting, the following antibodies were purchased from Cell Signalling Technologies IRF4 (Cat#4948; P173), STAT1 (Cat#9172T), STAT3 (Cat#4904), STAT4 (Cat#2653), STAT5a

(Cat#94205), STAT6 (Cat#5397), pSTAT1 Y701 (Cat#7649), pSTAT3 Y705 (Cat#9131), pSTAT4 Y693(Cat#5267), pSTAT5 Y694 (Cat#9351) and pSTAT6 Y641 (Cat#9361). Antibodies against STAT2 (Cat#ab134192) and pSTAT2 Y690 (Cat#ab53132) were from Abcam. The antibody for ShcA was from BD Transduction Laboratories (Cat#S14603). The antibody for BATF3 was from R and D Systems (Cat#AF7437). Antibody against Myb is from Sigma-Aldrich (Cat#05-175, Clone 1-1), Anti-ZEB2 was from Novus Biologicals (Cat#NBP1-82991) and Anti-BLIMP1 was from eBioscience (6D3). Anti-PTPN2 (3E2) was produced in-house [7], Anti-PTPN1 was from Upstate (EMD Millipore, Cat#07-088) and Anti-Calnexin (CNX) was a gift from Dr. John J.M. Bergeron. PTPN2/PTPN1 specific phosphatase small molecule inhibitors L598 and KQ791 were kindly donated by Kanyr Inc.

Cell purification and CTL differentiation

Cell isolation from splenocytes was performed with StemCell Technologies kits for CD4 (Cat#18952), CD8 (Cat#18953), and CD8 naïve (Cat#18958) following the manufacturer's instructions. Purified naïve CD8 T cells were seeded on non-tissue culture treated 24 well plates coated with 2mg/ml αCD3ε (Ultra LEAF© purified, clone145-2C11, Biolegend) at $2x10^5$ cells per well, in complete RPMI (RPMI 1640, 10% heat-inactivated FBS, 0.05mM β-mercaptoethanol and 1X Penicillin/Streptomycin Gibco) soluble αCD28 (Ultra LEAF© purified, clone 37.51, Biolegend) and 20U/ml recombinant murine interleukin 2 (rmIL-2) (Peprotech, cat. number 212-12). For stimulation with the cognate OVA 257-264 peptide (SIINFEKL), 2.5×10^5 splenocytes from OT-1 mice were seeded in one ml of complete media in 24 well plates and 0.5µg/ml of peptide (Sigma-Aldrich, cat. number S7951). After 48 hours blasts were expanded with 100 U/ml of rmIL-2 in fresh media and harvested on day 4 or day 6 after initial stimulation.

In experiments where pharmacological inhibitors were used a 10mM stock solution in PBS was added to the media at the appropriate final concentration, and an equal volume of PBS was added to the control cells. The fresh inhibitor was added every 48hs at the corresponding concentrations.

Flow cytometry

Spleen, lymph node, and thymus samples were prepared by macerating organs through a 70µm cell strainer (Falcon) to obtain a single-cell suspension, samples were kept on ice in 2%FBS PBS during the staining procedures. For intracellular staining of nuclear factors, samples were processed with the FOXP3/Transcription Factor Staining Buffer Set (eBioscience, Thermo-Fisher) following the manufacturer's instructions. Samples were read in a BD LSR Fortessa instrument and analyzed with FlowJo software.

Human T cell isolation and invitro expansion

Peripheral blood mononuclear cells (PBMCs) of healthy donors were obtained after informed consent approved by the local ethics committee (Hôpital Maisonneuve-Rosemont, Montreal, Québec; protocol #2020-2141) by venipuncture followed by manual (Ficoll-Paque, GE Healthcare, Canada) gradient density separation. T cells are isolated using an EasySep™ Human T Cell Enrichment Kit as described by the manufacturer (Stemcell Technologies). For T cell activation, 96 well plates were coated with anti-CD3 (Clone #145-2C11, BD Biosciences) antibody at 5µg/mL for 1h30 at 37C. After washing with PBS, 100,000 PBMC per well were seeded in complete media (Advanced RPMI with 10% human serum and 1% L-Glutamine) supplemented with 1µg/mL of anti-CD28 antibody (Clone #37.51, BD Biosciences). The L598 compound was added to the cultures every 2 days at 2, 5, 10, or 25µM. After 7 days, cells are harvested for analysis. Phenotypic evaluation of T cells is performed to determine the differentiation status. For functional analysis, T cells were incubated in 96 well plates with Brefeldin A (15µg/mL, Biolegend) and stimulated

with PMA (5ng/mL, Sigma) and Ionomycin (500ng/mL, Sigma) for 4 hours at 37C. Cells were then harvested, stained for extracellular markers, and then permeabilized (eBioscience™ Foxp3 / Transcription Factor Staining Buffer Set) overnight at 4C. After permeabilization, cells were washed and stained with TNF-α and IFN-γ antibodies to determine cytokine production following stimulation. Flow cytometry acquisition was performed on the BD LSRII instrument.

Invitro CTL-specific cytotoxicity

For specific cell cytotoxicity, a flow cytometry-based assay was used. EG.7 target cells were stimulated 24 hours before the experiment with 100 U/ml of rmIFN-γ to increase the expression of Class I molecules. OT-1 CD8 T cells were activated/expanded as mentioned above and harvested on day 4 for experiments. In experiments involving pharmacological inhibitors, cells were washed twice with media to prevent any side effects on target cells. EG.7 target cells were loaded with CellTracker™ Orange CMRA dye (ThermoFisher Scientific) for 30 min, following the manufacturer's instructions, and after being washed extensively with serum-containing media to inactivate the dye remaining in the solution. After, CD8 effector and EG.7 target cells were plated at the corresponding ratios in round bottom 96 well plates, centrifuged at 300g for 2 min, and incubated a 37˚C and 5% CO2 for 5 hours. Some wells were plated with target cells alone to be used as spontaneous dead controls. Following incubation, cocultures were centrifuged for 5 minutes at 300g and the supernatant was harvested for cytokine quantification. Cocultures were then washed with PBS and stained with LIVE/DEAD™ Fixable Blue Dead Cell Stain Kit or LIVE/DEAD™ Fixable Aqua Dead Cell Stain Kit (ThermoFisher Scientific) following the manufacturer's instructions. Cocultures were then incubated for 30 minutes protected from light and washed twice with 2%FBS PBS. After the last wash cocultures were either read immediately or fixed with 2% PFA in PBS for 45 min, washed, and resuspended in 2%FBS PBS. Samples were

acquired in BD LSR Fortessa or BD Canto machines and analyzed with FlowJo software. The target cell death percentage was calculated as the percentage of LIVE/DEAD stain-positive cells from the CMRA-positive events. To calculate specific target cell cytotoxicity, spontaneous cell death was subtracted from that observed in experimental samples. Values correspond to the average of technical replicates. This protocol was optimized to obtain a non-saturated curve from the samples with the highest activity (N2KO/N1Het and dKO CTLs), hence the lower values obtained with CRE controls.

CTL stimulation with INF-β, protein extraction, and immunoblotting

To evaluate protein phosphorylation in CD8 T cells after stimulation with IFN-β (Peprotech), day 4 CTL were washed twice in serum-free media and incubated for 2 hours under serum and cytokine deprivation before stimulation, serum-free media was maintained during stimulations. To stop stimulation cells were lysed by adding an equal volume of ice-cold 2X RIPA buffer (100 mm Tris–HCl pH 7.4, 200 mm NaCl, 0.2 mm EDTA, 2% NP40, 0.2% SDS) containing protease (Roche complete protease inhibitor cocktail, Sigma-Aldrich) and phosphatase inhibitors (4mM sodium orthovanadate, 10mM NaF, 20 mM sodium pyrophosphate). Lysates were then migrated through 10 or 12% PAGE and transferred to PVDF membranes (Immobilon-P, EMD Millipore).

Primary CD8 T cells siRNA knockdown

After day 2 of expansion, 5 x 10^6 N2KO/N1Het CTLs were nucleofected with ON-TARGET plus SMARTpool short interfering RNAs (siRNA) specific for BatF3 purchased from Dharmacon. ON-TARGETplus Non-targeting Pool was used as control. P3 Primary Cell 4D-Nucleofector™ X Kit (Cat#V4XP-3032, Lonza Cologne) and the AMAXA Nucleofector System program CY-100 for primary cells were used according to the manufacturer's instructions. After pulsation, cells were

placed back in culture in media complemented with 20U/ml rail-2 (Peprotech) and harvested for experiments on day 5.

ELISA

To measure cytokine secretion in supernatants from cytotoxicity experiments, enzyme-linked immunoassays (ELISA) for mouse IFN-γ Biolegend (Cat#430804) and IL-10 ThermoFisher (Cat#88-7105-88) were used according to manufacturer's instructions.

mRNA isolation

To reduce potential variations given by the differentiation state of splenic CD8 T cells, mRNA for bulk sequencing experiments was isolated from day 4 CTLs expanded from purified splenic naïve CD8 T cells. For each sample, 2x 10^6 cells were processed under laminar flow cabinets with the RNAEasy plus mini from Qiagen (Cat# 74134) following the manufacturer's instructions.

Gene expression profiling

After RNA extraction, libraries for sequencing were prepared using the Illumina TruSeq RNA Library Prep Kit following the manufacturer's instructions. High throughput sequencing was performed at the Centre d'expertise et de services Génome Québec. 28 to 46 million reads were obtained per sample, with an average of 35 million reads.

mRNA sequencing data processing

The resulting reads were aligned to the GRCm38 mouse reference genome assembly, using STAR [53]. SAM files were sorted with samtools 1.10. Read counts were obtained using HTSeq [54] with parameters -m intersection-nonempty -stranded=reverse.

For all downstream analyses, we excluded lowly-expressed genes with an average read count lower than 10 across all samples. Raw counts were normalized using edgeR's TMM algorithm

[55] and were then transformed to log2-counts per million (log CPM) using the voom function implemented in the limma R package [56]. To assess differences in gene expression levels, we fitted a linear model using limma's lmfit function. Nominal p-values were corrected for multiple testing using the Benjamini-Hochberg method. Gene set enrichment analyses were performed using Enrichr [57]. Volcano/dot plots and heatmaps were created using the R package ggplot2 and ComplexHeatmap, respectively.

Tumor inoculation and immunotherapy models

For immunotherapy models, 8-10 weeks old C57BL/6 males were purchased from The Jackson laboratory. Mice were shaved in the right flank and 3 x 10^5 B16F10 or E.G7 cells were injected in 100 µl of PBS. Tumor volume was calculated by measuring 2 axes (length and width) and applying the formula V = 4/3π × [(Length/2) × (Width/2)2]. For treatment by intratumoral injections in the E.G7 model, after reaching at least 50 mm3 tumors were injected with 1:20 volume of an L598 solution at 10mM in PBS (equivalent to a 50 µM L598 dose) every 2 days. For systemic treatment in the B16F10 model, intraperitoneal injections of KQ-791 at 10µg/g of weight and/or 100µg of anti-PD-1 antibody, Bio X Plus (Clone RPM1-14; Cat# BP0146) were started at day 2 post tumor inoculation. KQ-791 (kind gift from Kanyr Pharma Inc.) injections were repeated every 2 days for a total of 5 doses, and anti-PD-1 injections were repeated every 3 days for a total of 3 doses. In both models, humane intervention for euthanasia followed McGill University Research and Ethics Animal committee guidelines, including tumor volume reaching 2000 mm3, tumor ulceration or deterioration of the clinical condition. Only mice reaching humane endpoint by tumor volume were included in the experiments.

Invitro phosphatase assay

Enzyme reactions were conducted in assay buffer 50mM HEPES pH7.0, 3mM DTT and 1mg/mL BSA using the purified recombinant GST-PTP1B and GST-TC-PTP catalytic domains [58]. DiFMUP was used as a substrate.

Determination of kinetics constants using DiFMUP as substrate: The hydrolysis of DiFMUP was conducted in black 96-well plates (Corning) in a final volume of 100µL at 25°C. The reaction was monitored by measuring the fluorescence (excitation wavelength 358nm/emission 455nm) with the Varioskan plate reader (Thermo Electron). Enzyme dilution was determined by choosing a reaction rate to comprise in an Absorbance range of 5-30 FU units/min. For the kinetic assays fluorescence was monitored over 10 minutes in 30 seconds intervals and rates were calculated using a non-linear least-square fitting procedure. Km was determined from rates at various substrate concentrations using the Michaelis-Menten equation and IC50 values were derived by a sigmoidal dose-response (variable slope) curve using GraphPad Prism software. A substrate concentration equivalent to the Km value was used for IC50 determinations. KQ-791 and L598 Inhibitors were diluted in PBS, and then a serial dilution starting from 24µM and covering 3 log scales was made in assay buffer.

Statistical analysis

All statistical analyses were performed using GraphPad Prism software.

References

1. Pike, K.A. and M.L. Tremblay, *TC-PTP and PTP1B: Regulating JAK-STAT signaling, controlling lymphoid malignancies.* Cytokine, 2016. **82**: p. 52-7.
2. Penafuerte, C., et al., *Downregulation of PTP1B and TC-PTP phosphatases potentiate dendritic cell-based immunotherapy through IL-12/IFNγ signaling.* OncoImmunology, 2017. **6**(6): p. e1321185.
3. Manguso, R.T., et al., *In vivo CRISPR screening identifies Ptpn2 as a cancer immunotherapy target.* Nature, 2017. **547**: p. 413.

4. LaFleur, M.W., et al., *PTPN2 regulates the generation of exhausted CD8+ T cell subpopulations and restrains tumor immunity.* Nature Immunology, 2019. **20**(10): p. 1335-1347.
5. Wiede, F., et al., *PTPN2 phosphatase deletion in T cells promotes anti-tumour immunity and CAR T-cell efficacy in solid tumours.* The EMBO Journal, 2019. **n/a**(n/a): p. e103637.
6. Wiede, F., et al., *PTP1B Is an Intracellular Checkpoint that Limits T-cell and CAR T-cell Antitumor Immunity.* Cancer Discovery, 2022. **12**(3): p. 752-773.
7. You-Ten, K.E., et al., *Impaired Bone Marrow Microenvironment and Immune Function in T Cell Protein Tyrosine Phosphatase–deficient Mice.* Journal of Experimental Medicine, 1997. **186**(5): p. 683-693.
8. Wiede, F., et al., *Strain-Dependent Differences in Bone Development, Myeloid Hyperplasia, Morbidity and Mortality in Ptpn2-Deficient Mice.* PLOS ONE, 2012. **7**(5): p. e36703.
9. Bourdeau, A., et al., *TC-PTP-deficient bone marrow stromal cells fail to support normal B lymphopoiesis due to abnormal secretion of interferon-{gamma}.* Blood, 2007. **109**(10): p. 4220-8.
10. Bourdeau, A., et al., *Inhibition of T Cell Protein Tyrosine Phosphatase Enhances Interleukin-18-Dependent Hematopoietic Stem Cell Expansion.* STEM CELLS, 2013. **31**(2): p. 293-304.
11. Elchebly, M., et al., *Increased Insulin Sensitivity and Obesity Resistance in Mice Lacking the Protein Tyrosine Phosphatase-1B Gene.* Science, 1999. **283**(5407): p. 1544-1548.
12. Dubé, N., et al., *Genetic Ablation of Protein Tyrosine Phosphatase 1B Accelerates Lymphomagenesis of p53-Null Mice through the Regulation of B-Cell Development.* Cancer Research, 2005. **65**(21): p. 10088-10095.
13. Heinonen, K.M., et al., *Protein tyrosine phosphatase 1B negatively regulates macrophage development through CSF-1 signaling.* Proceedings of the National Academy of Sciences of the United States of America, 2006. **103**(8): p. 2776-2781.
14. Le Sommer, S., et al., *Deficiency in Protein Tyrosine Phosphatase PTP1B Shortens Lifespan and Leads to Development of Acute Leukemia.* Cancer Research, 2018. **78**(1): p. 75-87.
15. Berdnikovs, S., et al., *PTP1B Deficiency Exacerbates Inflammation and Accelerates Leukocyte Trafficking In Vivo.* The Journal of Immunology, 2012. **188**(2): p. 874-884.
16. Heinonen, K.M., et al., *Protein tyrosine phosphatases PTP-1B and TC-PTP play nonredundant roles in macrophage development and IFN-γ signaling.* Proceedings of the National Academy of Sciences, 2009. **106**(23): p. 9368-9372.
17. Klaman, L.D., et al., *Increased Energy Expenditure, Decreased Adiposity, and Tissue-Specific Insulin Sensitivity in Protein-Tyrosine Phosphatase 1B-Deficient Mice.* Molecular and Cellular Biology, 2000. **20**(15): p. 5479-5489.
18. Hashimoto, M., et al., *CD8 T Cell Exhaustion in Chronic Infection and Cancer: Opportunities for Interventions.* Annual Review of Medicine, 2018. **69**(1): p. 301-318.
19. Galon, J., et al., *Type, Density, and Location of Immune Cells Within Human Colorectal Tumors Predict Clinical Outcome.* Science, 2006. **313**(5795): p. 1960-1964.
20. Kmiecik, J., et al., *Elevated CD3+ and CD8+ tumor-infiltrating immune cells correlate with prolonged survival in glioblastoma patients despite integrated immunosuppressive mechanisms in the tumor microenvironment and at the systemic level.* Journal of Neuroimmunology, 2013. **264**(1): p. 71-83.
21. Djenidi, F., et al., *CD8⁺CD103⁺ Tumor–Infiltrating Lymphocytes Are Tumor-Specific Tissue-Resident Memory T Cells and a Prognostic Factor for Survival in Lung Cancer Patients.* The Journal of Immunology, 2015. **194**(7): p. 3475-3486.
22. Dudley, M.E., et al., *Cancer Regression and Autoimmunity in Patients After Clonal Repopulation with Antitumor Lymphocytes.* Science, 2002. **298**(5594): p. 850-854.

23. Berger, C., et al., *Adoptive transfer of effector CD8+ T cells derived from central memory cells establishes persistent T cell memory in primates.* The Journal of Clinical Investigation, 2008. **118**(1): p. 294-305.
24. Rosenberg, S.A., et al., *Durable Complete Responses in Heavily Pretreated Patients with Metastatic Melanoma Using T-Cell Transfer Immunotherapy.* Clinical Cancer Research, 2011. **17**(13): p. 4550-4557.
25. Haslam, A., J. Gill, and V. Prasad, *Estimation of the Percentage of US Patients With Cancer Who Are Eligible for Immune Checkpoint Inhibitor Drugs.* JAMA Network Open, 2020. **3**(3): p. e200423-e200423.
26. Waldman, A.D., J.M. Fritz, and M.J. Lenardo, *A guide to cancer immunotherapy: from T cell basic science to clinical practice.* Nature Reviews Immunology, 2020. **20**(11): p. 651-668.
27. Townsend, E.C., et al., *The Public Repository of Xenografts Enables Discovery and Randomized Phase II-like Trials in Mice.* Cancer Cell. **29**(4): p. 574-586.
28. Penafuerte, C., et al., *Mining the Complex Family of Protein Tyrosine Phosphatases for Checkpoint Regulators in Immunity*. 2017, Springer Berlin Heidelberg: Berlin, Heidelberg. p. 1-24.
29. Bussières-Marmen, S., et al., *Loss of T-cell protein tyrosine phosphatase in the intestinal epithelium promotes local inflammation by increasing colonic stem cell proliferation.* Cellular & Molecular Immunology, 2018. **15**(4): p. 367-376.
30. Zee, T., et al., *T-Cell Protein Tyrosine Phosphatase Regulates Bone Resorption and Whole-Body Insulin Sensitivity through Its Expression in Osteoblasts.* Molecular and Cellular Biology, 2012. **32**(6): p. 1080-1088.
31. Maekawa, Y., et al., *Notch2 integrates signaling by the transcription factors RBP-J and CREB1 to promote T cell cytotoxicity.* Nature Immunology, 2008. **9**: p. 1140.
32. Pépin, G., et al., *Cre-dependent DNA recombination activates a STING-dependent innate immune response.* Nucleic Acids Research, 2016. **44**(11): p. 5356-5364.
33. Carow, B., et al., *lck-Driven Cre Expression Alters T Cell Development in the Thymus and the Frequencies and Functions of Peripheral T Cell Subsets.* The Journal of Immunology, 2016: p. 1600827.
34. Doering, Travis A., et al., *Network Analysis Reveals Centrally Connected Genes and Pathways Involved in CD8⁺ T Cell Exhaustion versus Memory.* Immunity, 2012. **37**(6): p. 1130-1144.
35. Hogquist, K.A., et al., *T cell receptor antagonist peptides induce positive selection.* Cell, 1994. **76**(1): p. 17-27.
36. Vidović, D. and S.C. Schürer, *Knowledge-Based Characterization of Similarity Relationships in the Human Protein−Tyrosine Phosphatase Family for Rational Inhibitor Design.* Journal of Medicinal Chemistry, 2009. **52**(21): p. 6649-6659.
37. Lau, C.K., et al., *Structure based design of a series of potent and selective non peptidic PTP-1B inhibitors.* Bioorganic & Medicinal Chemistry Letters, 2004. **14**(4): p. 1043-1048.
38. Montalibet, J., et al., *Residues Distant from the Active Site Influence Protein-tyrosine Phosphatase 1B Inhibitor Binding.* Journal of Biological Chemistry, 2006. **281**(8): p. 5258-5266.
39. Agarwal, P., et al., *Gene Regulation and Chromatin Remodeling by IL-12 and Type I IFN in Programming for CD8 T Cell Effector Function and Memory.* The Journal of Immunology, 2009. **183**(3): p. 1695-1704.
40. Marshall, H.D., et al., *IFN-αβ and Self-MHC Divert CD8 T Cells into a Distinct Differentiation Pathway Characterized by Rapid Acquisition of Effector Functions.* The Journal of Immunology, 2010. **185**(3): p. 1419-1428.
41. Platanias, L.C., *Mechanisms of type-I- and type-II-interferon-mediated signalling.* Nature Reviews Immunology, 2005. **5**: p. 375.

42. Danilo, M., et al., *Suppression of Tcf1 by Inflammatory Cytokines Facilitates Effector CD8 T Cell Differentiation.* Cell Reports, 2018. **22**(8): p. 2107-2117.
43. Spalinger, M.R., et al., *PTPN2 controls differentiation of CD4+ T cells and limits intestinal inflammation and intestinal dysbiosis.* Mucosal Immunol, 2015. **8**(4): p. 918-929.
44. Chen, J., et al., *NR4A transcription factors limit CAR T cell function in solid tumours.* Nature, 2019. **567**(7749): p. 530-534.
45. Spranger, S., et al., *Tumor-Residing Batf3 Dendritic Cells Are Required for Effector T Cell Trafficking and Adoptive T Cell Therapy.* Cancer Cell, 2017. **31**(5): p. 711-723.e4.
46. Ataide, M.A., et al., *BATF3 programs CD8+ T cell memory.* Nature Immunology, 2020. **21**(11): p. 1397-1407.
47. Miller, B.C., et al., *Subsets of exhausted CD8+ T cells differentially mediate tumor control and respond to checkpoint blockade.* Nature Immunology, 2019. **20**(3): p. 326-336.
48. McLane, L.M., M.S. Abdel-Hakeem, and E.J. Wherry, *CD8 T Cell Exhaustion During Chronic Viral Infection and Cancer.* Annual Review of Immunology, 2019. **37**(1): p. 457-495.
49. Seo, H., et al., *TOX and TOX2 transcription factors cooperate with NR4A transcription factors to impose CD8⁺ T cell exhaustion.* Proceedings of the National Academy of Sciences, 2019. **116**(25): p. 12410-12415.
50. Khan, O., et al., *TOX transcriptionally and epigenetically programs CD8+ T cell exhaustion.* Nature, 2019. **571**(7764): p. 211-218.
51. Scott, A.C., et al., *TOX is a critical regulator of tumour-specific T cell differentiation.* Nature, 2019. **571**(7764): p. 270-274.
52. Flosbach, M., et al., *PTPN2 Deficiency Enhances Programmed T Cell Expansion and Survival Capacity of Activated T Cells.* Cell Reports, 2020. **32**(4): p. 107957.
53. Dobin, A., et al., *STAR: ultrafast universal RNA-seq aligner.* Bioinformatics, 2012. **29**(1): p. 15-21.
54. Anders, S., P.T. Pyl, and W. Huber, *HTSeq—a Python framework to work with high-throughput sequencing data.* Bioinformatics, 2014. **31**(2): p. 166-169.
55. Robinson, M.D., D.J. McCarthy, and G.K. Smyth, *edgeR: a Bioconductor package for differential expression analysis of digital gene expression data.* Bioinformatics, 2009. **26**(1): p. 139-140.
56. Ritchie, M.E., et al., *limma powers differential expression analyses for RNA-sequencing and microarray studies.* Nucleic Acids Research, 2015. **43**(7): p. e47-e47.
57. Kuleshov, M.V., et al., *Enrichr: a comprehensive gene set enrichment analysis web server 2016 update.* Nucleic Acids Research, 2016. **44**(W1): p. W90-W97.
58. Stuible, M., et al., *Cellular Inhibition of Protein Tyrosine Phosphatase 1B by Uncharged Thioxothiazolidinone Derivatives.* ChemBioChem, 2007. **8**(2): p. 179-186.

Figure legends.

Figure 1. CD8 T cell activation and differentiation are increased in naïve mice with reduced expression of PTPN2 and/or PTPN1. Ex vivo analysis of peripheral T cells populations of naïve 6 to 8 weeks old mice with conditional deletions of *Ptpn1* and/or *Ptpn2* in mature post-thymic CD8 T cells by multiparametric flow cytometric analysis of T cells. A) Panels of CD4 vs CD8 cells from different genotypes. Events shown correspond to single, viable, and lineage-negative (Lin-) gates. B) Statistical representation of T cell subtypes from different experiments organized by genotype, C) Histogram representation, and D) Quantification of CD8 low populations observed in the spleen of different genotypes. E) Dot plots and F) Statistical representation of CD8 T cell differentiation from spleen and lymph nodes, determined by CD62L and CD44 expression; naïve cells are defined as CD62L high and CD44 low, T central memory (Tcm) defined as CD62L high and CD44 high cells, and T effector/effector (Teff/eff) memory as CD62L low and CD44 intermediate cells. G) Histogram representation and H) Quantification of differentiation markers EOMES, KLRG1, and CD127. (CRE n=4, N1KO n=2, N2KO n=4, N2KO/N1Het n=2, dKO n=4) (Bars represent +/- S.E.M.; non-parametric Kruskal-Wallis test (D) or Mixed-effects analysis (B, F, H); P values *<0.05, **<0.005, ***<0.0005, ****<0.00005).

Figure 2. Mouse CD8 T cells deficient in PTPN2 and/or PTPN1 are more cytotoxic and reach terminal differentiation. Naïve CD8 T cells from the spleen of mice with different *Ptpn1* and/or *Ptpn2* deletions, expressing E8i-CRE and the OT-1 TCR, were activated/expanded with αCD3/αCD28 antibodies and IL-2 to generate CTL. A) Day 4 CTL were tested in vitro for specific cytotoxicity against the OVA-expressing thymoma E.G7 cells. B) Statistical representation of several experiments from (A). C) ELISA quantification of mouse IFN-γ in supernatants from (A). D) and E) CD8 T cell differentiation determined by flow cytometric analysis of CD62L and CD44

expression. D) Flow cytometry plots of cells gated in singlet/ live events. E) Bar representation of the percentages of different populations from several experiments from (D). (All data representative of at least 3 different biological replicates; bars represent +/- S.E.M.; non-parametric Kruskal-Wallis test (B) or Mixed-effects analysis (C, E); P values *<0.05, **<0.005, ***<0.0005, ****<0.00005).

Figure 3. Pharmacological inhibition of PTPN2 and PTPN1 results in enhanced cytotoxicity and effector differentiation. CD8 T cells from OT-1 mice were activated/expanded by αCD3/αCD28 antibodies and IL-2 in the presence of different concentrations of PTPN2/PTPN1 inhibitor L598 for 4 days. A) Specific cytotoxicity against OVA expressing thymoma E.G7 cells. B) Statistical representation of several experiments. (n=4) C) ELISA quantification of IFN-γ in supernatants from (A). D) and E) CD8 T cell differentiation determined by flow cytometric analysis of CD62L and CD44 expression in cells from (A). D) Flow cytometry plots of cells gated in singlet/ events. E) Bar representation of Tcm population percentages from different animals. (n=3) F) Specific cytotoxicity against E.G7 cells of CD8 T cells from animals with different PTPN2 and PTPN1 genotypes, additionally treated with L598 during expansion/differentiation. G) ELISA quantification of IFN-γ in supernatants from (F) (Bars represent +/- S.E.M.; One-way (E) or Two-way (B, C, G) ANOVA; P values *<0.05, **<0.005, ***<0.0005, ****<0.00005).

Figure 4. Pharmacological inhibition of PTPN2 and PTPN1 in human T cells results in enhanced proinflammatory cytokine secretion and Tcm differentiation. Purified T cells from human donors were activated by αCD3/αCD28 and analyzed on day 7 for IFN-γ and TNF-α by flow cytometric analysis. A) Plots of cells gated in CD4 and CD8 populations distributed by IFN-γ and TNF-α expression. B) and C) Bar graphs showing the statistical representation of 2 biological

replicates. D) Bar graphs of cell populations sorted by expression of CD45RO and CD62L defining Tem ($CD45RO^{high}$; $CD62L^{low}$) and Tcm ($CD45RO^{high}$; $CD62L^{high}$) phenotypes.

Figure 5. Global changes of STAT expression and phosphorylation in CD8 T cells with reduced or absent PTPN2/PTPN1 activity. A) and C) Immunoblotting of protein lysates from day 4 CTL, serum, and cytokine starved for 2 hours and stimulated with 5000 Units of recombinant murine interferon β (rmIFN-β) for the indicated times. Controls correspond to cells without the addition of the cytokine. B) Densitometric analysis of data represented in (A). Total protein expression was normalized to the expression of the adaptor protein ShcA. (Representative of at least 3 independent experiments).

Figure 6. Bulk mRNA analysis of CD8 T cells deficient in PTPN2 and/or PTPN1 or treated with L598. A) Principal component analysis (PCA) of bulk mRNA sequencing samples obtained from day 4 CTL from different genotypes. B) Volcano plot illustrating the significant differentially expressed genes between N2KO and N2KO/N1 Het genotypes (FDR 5%), in blue significantly downregulated genes (Downreg), in red significantly upregulated genes (Upreg). C) Dot plot corresponding to a selected list of genes relevant to CD8 T cells activation/differentiation. Overexpressed genes showed a gradual red shift, and under-expressed genes a gradual blue shift.

Figure 7. Increased expression of transcription factors in CD8T cells with reduced or absent PTPN2/PTPN1 activity. Immunoblot analysis of cell homogenates from the day 4 CTL of the different genotypes was analyzed and probed with antibodies for the indicated transcription factors. Expression of PTPN1 and PTPN2 was also assessed by immunoblot. As a loading control, membranes were probed for calnexin. (Representative of at least 2 different experiments).

Figure S1. Conditional deletion of PTPN2 and PTPN1 in CD8 T cells. A) Breeding schematics showing the steps to obtain the different genotypes analyzed. B) Immunoblot for PTPN2, PTPN1, and Calnexin as loading control from protein homogenates of CD4 and CD8 T cells with different genotypes analyzed. C) Thymus size, expressed as weight, from 8–12-week-old male mice carrying the different genotypes analyzed. D) Hematoxylin and eosin staining of thymus sections from 10-week-old CRE controls or PTPN2/PTPN1 (dKO) CD8 specific "knockouts". E) Spleen and inguinal lymph node size (by weight) and cellularity from the different genotypes analyzed. F) Total number of CD4 and CD8 T cells from spleen and inguinal lymph nodes shown in Figure N1, no significant differences were found. (Bars represent +/- S.E.M.; Kruskal-Wallis test (C, E) or Two-way (F); P values *<0.05, **<0.005, ***<0.0005, ****<0.00005).

Figure S2. In vitro cytotoxicity against specific target cells of CD8 T cells with genetic deficiency of PTPN2 and/or PTPN1. A) Purified naïve CD8 T cells from C57Bl/6 WT or OT-1 mice were stimulated to generate CTL either by receptor crosslinking of CD3 and CD28 with specific antibodies, and IL-2 (leftmost and central plots) or with cognate peptide and APC (right plot). Cells were analyzed by flow cytometry for the expression of the TCR variable alpha chain 2 and TCR beta variable chain 5.1. Cells expressing the transgenic chains in the OT-1 mouse are positive for both (Q6) B) Statistical representation of day 4 CTLs from all the different genotypes tested for specific cytotoxicity against the OVA expressing E.G7 thymoma cells. Each panel represents a different effector to target ratio, to simplify statistical differences, panels for 5:1, 10:1, and 20: ratios show comparisons of all groups to CRE and N2KO groups (Bars represent +/- S.E.M.; Kruskal-Wallis test; P values *<0.05, **<0.005, ***<0.0005, ****<0.00005) C) Correlation plot of effector memory/effector differentiation against cytotoxic activity against E.G7 cells at 10 to 1 ratio for the different genotypes analyzed. Spearman's rank correlation was

computed to assess the relationship between both variables, no correlation was observed (r=0.3, p=0.3417).

Figure S3. OT-1 Naïve CD8 T cells activated with the cognate peptide behave as those stimulated by antibody cross-linking. Splenocytes from OT-1 mice were stimulated with the OVA peptide 257-264 (SIINFEKL) for 2 days and later expanded with IL-2 in the presence of 10µM L598 or the vehicle (PBS) as control. A) Day 4 and day 6 CTL were tested for specific cytotoxicity against E.G7 OVA-expressing thymoma cells. B) Cells in A were assessed for expression of the differentiation markers CD62L and CD44. (Representative of 2 different experiments)

Figure S4. Pharmacological inhibition of PTPN2 and PTPN1 in human T cells. The normalized percentual representation of experiments in Figure 3 shows A) IFN-γ and B) TNF-α. C) Percentual contribution of CD4 and CD8 T cells of in vitro human T cell cultures at day 7.

Figure S5. Bulk mRNA analysis of CD8 T cells deficient in PTPN2 and/or PTPN1 or treated with L598. Volcano plots represent A) the significant differentially expressed genes between day 4 CTLs from CRE controls and the different genotypes analyzed. B) Heatmap of genes differentially expressed in the genotypes analyzed and organized as opposing expression between N2KO/N1Het CD8 T cells and CRE controls. Overexpressed genes showed a gradual red shift, and under-expressed genes a gradual blue shift. C) Same data as in figure 6A, with the addition of samples from C57BL/6 mice CTL treated (B6.L598) or not (B6) with 5µM of L598 during differentiation/expansion. D) Differential expression of the different members of the NR4A transcription factor family from samples in (C).

Figure S6. Increased expression of transcription factors in CD8T cells with reduced or absent PTPN2/PTPN1 activity. A) Table listing the fold change of several transcription factors relevant in CD8 T cells differentiation and function (data from experiments in Figure 6). Significant differences are defined by a false discovery rate of 5%. B) Specific cytotoxicity against OVA expressing E.G7 thymoma cells from day 4 N2KO/N1Het CTLs transfected with no target or BATF3 siRNAs. C) Immunoblot with specific BATF3 and calnexin antibodies to demonstrate specific deletion. A) and B) representative of 3 independent experiments.

Supplementary Table 1. List of significant differentially expressed genes between day 4 activated CD8 T cells from N2KO vs. N2KO/N1Het.

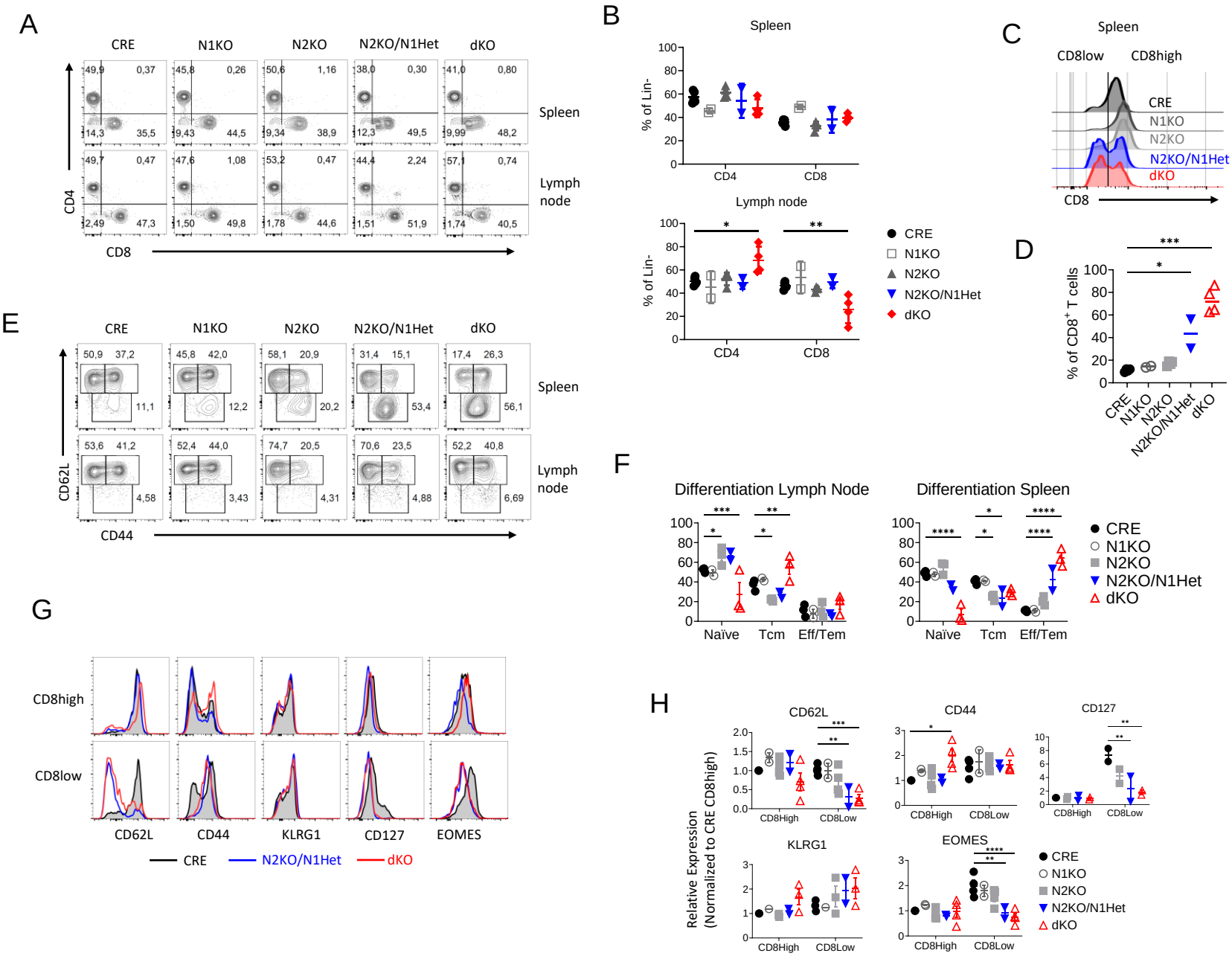
A
CRE
N1KO
N2KO
N2KO/N1Het
dKO
Spleen
Lymph node
CD4
CD8
B
Spleen
% of Lin-
CD4
CD8
Lymph node
CRE
N1KO
N2KO
N2KO/N1Het
dKO
C
Spleen
CD8low
CD8high
CRE
N1KO
N2KO
N2KO/N1Het
dKO
CD8
D
% of CD8+ T cells
CRE
N1KO
N2KO
N2KO/N1Het
dKO
E
CRE
N1KO
N2KO
N2KO/N1Het
dKO
Spleen
Lymph node
CD62L
CD44
F
Differentiation Lymph Node
Differentiation Spleen
Naïve
Tcm
Eff/Tem
CRE
N1KO
N2KO
N2KO/N1Het
dKO
G
CD8high
CD8low
CD62L
CD44
KLRG1
CD127
EOMES
CRE
N2KO/N1Het
dKO
H
CD62L
CD44
CD127
KLRG1
EOMES
Relative Expression
(Normalized to CRE CD8high)
CD8High
CD8Low
CRE
N1KO
N2KO
N2KO/N1Het
dKO

Figure 1

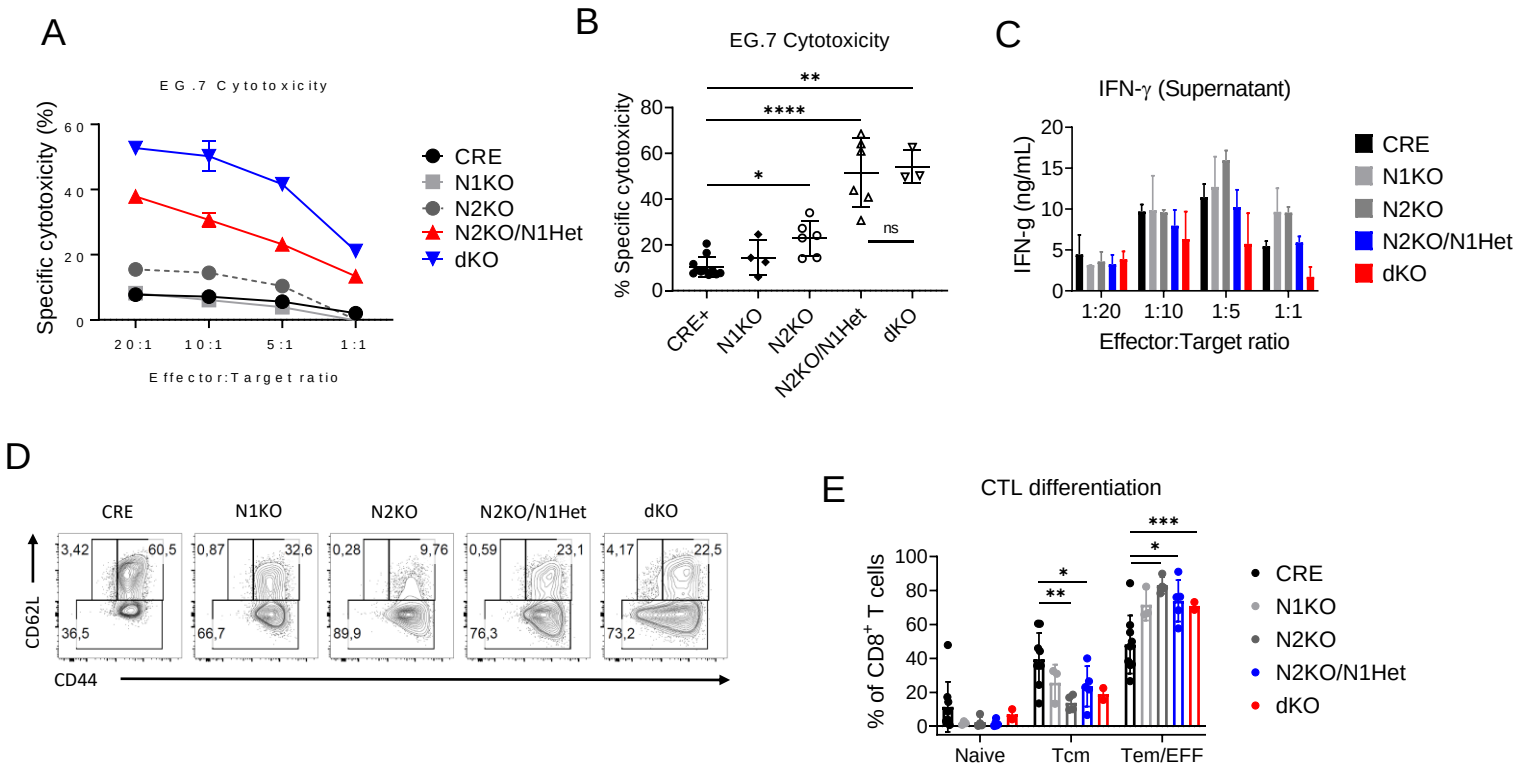
A
EG.7 Cytotoxicity
Specific cytotoxicity (%)
60
40
20
0
20:1
10:1
5:1
1:1
Effector:Target ratio
CRE
N1KO
N2KO
N2KO/N1Het
dKO
B
EG.7 Cytotoxicity
% Specific cytotoxicity
80
60
40
20
0
**
****
*
ns
CRE+
N1KO
N2KO
N2KO/N1Het
dKO
C
IFN-γ (Supernatant)
IFN-g (ng/mL)
20
15
10
5
0
1:20
1:10
1:5
1:1
Effector:Target ratio
CRE
N1KO
N2KO
N2KO/N1Het
dKO
D
CRE
N1KO
N2KO
N2KO/N1Het
dKO
CD62L
CD44
3,42
60,5
36,5
0,87
32,6
66,7
0,28
9,76
89,9
0,59
23,1
76,3
4,17
22,5
73,2
E
CTL differentiation
% of CD8+ T cells
100
80
60
40
20
0
*
**
***
*
Naive
Tcm
Tem/EFF
CRE
N1KO
N2KO
N2KO/N1Het
dKO

Figure 2

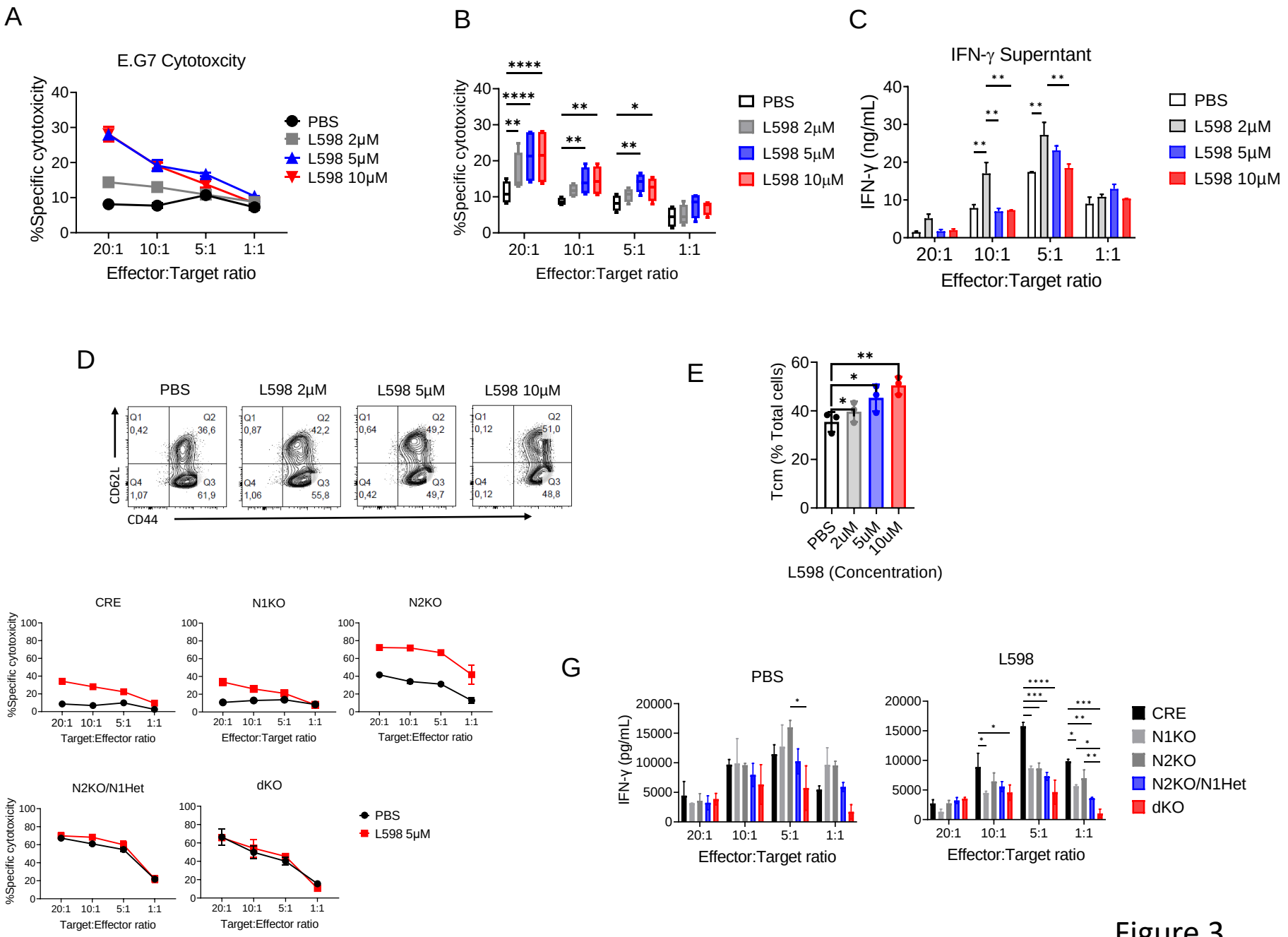
A
E.G7 Cytotoxcity
%Specific cytotoxicity
Effector:Target ratio
20:1
10:1
5:1
1:1
PBS
L598 2μM
L598 5μM
L598 10μM
B
%Specific cytotoxicity
Effector:Target ratio
C
IFN-γ Superntant
IFN-γ (ng/mL)
Effector:Target ratio
D
PBS
L598 2μM
L598 5μM
L598 10μM
CD62L
CD44
Q1 0,42
Q2 36,6
Q4 1,07
Q3 61,9
Q1 0,87
Q2 42,2
Q4 1,06
Q3 55,8
Q1 0,64
Q2 49,2
Q4 0,42
Q3 49,7
Q1 0,12
Q2 51,0
Q4 0,12
Q3 48,8
E
Tcm (% Total cells)
PBS
2uM
5uM
10uM
L598 (Concentration)
F
CRE
N1KO
N2KO
N2KO/N1Het
dKO
%Specific cytotoxicity
Target:Effector ratio
Effector:Target ratio
PBS
L598 5μM
G
PBS
L598
IFN-γ (pg/mL)
Effector:Target ratio
CRE
N1KO
N2KO
N2KO/N1Het
dKO

Figure 3

A

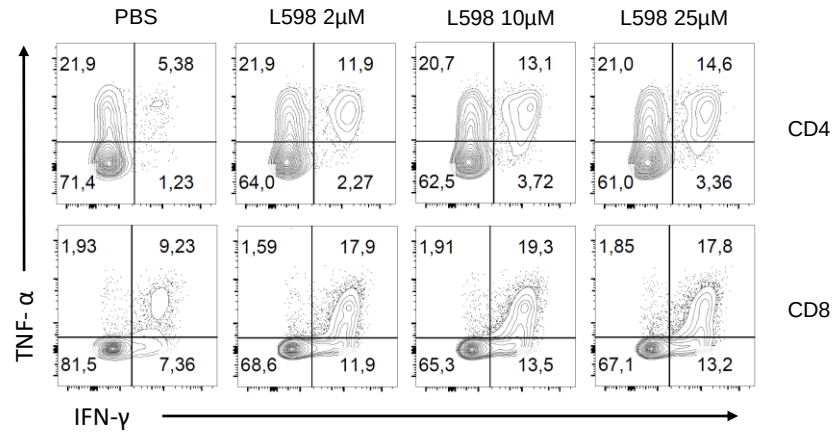

B

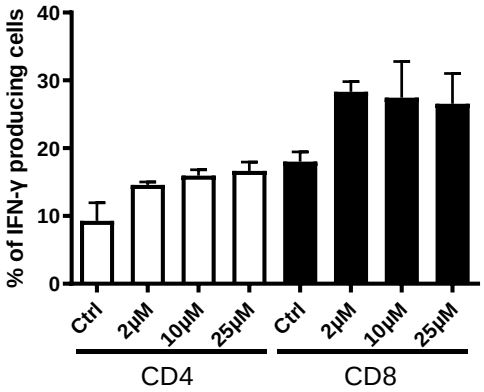

C

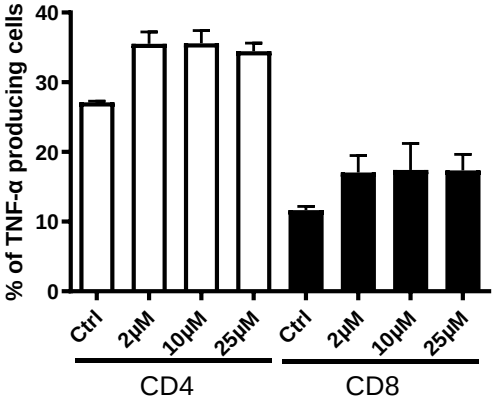

D

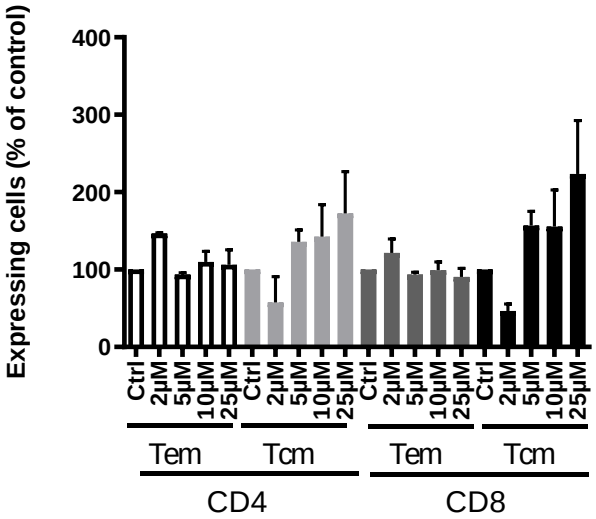

Figure 4

A

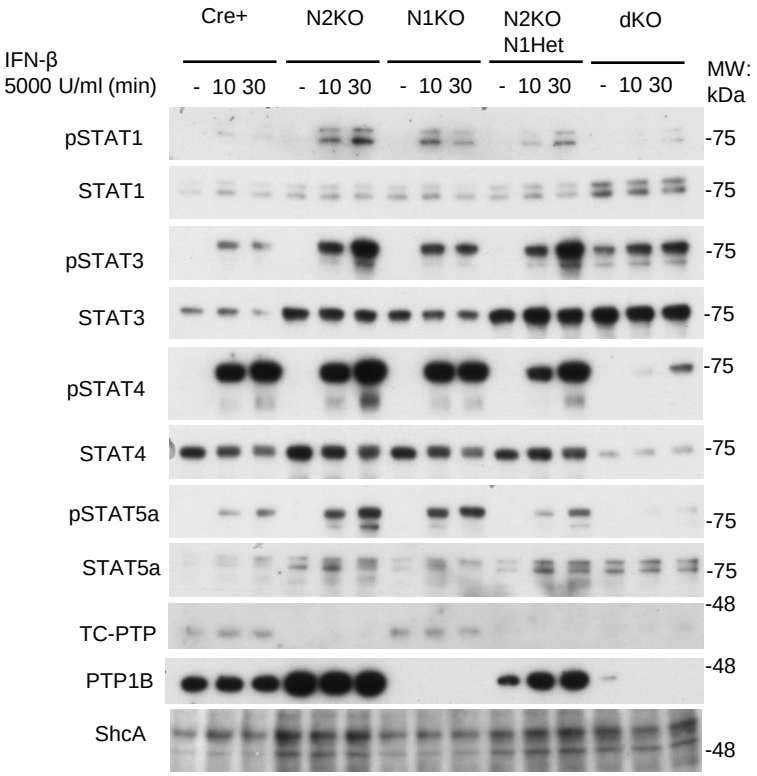
Cre+
N2KO
N1KO
N2KO N1Het
dKO
IFN-β 5000 U/ml (min)
- 10 30
MW: kDa
pSTAT1
STAT1
pSTAT3
STAT3
pSTAT4
STAT4
pSTAT5a
STAT5a
TC-PTP
PTP1B
ShcA
-75
-48

B

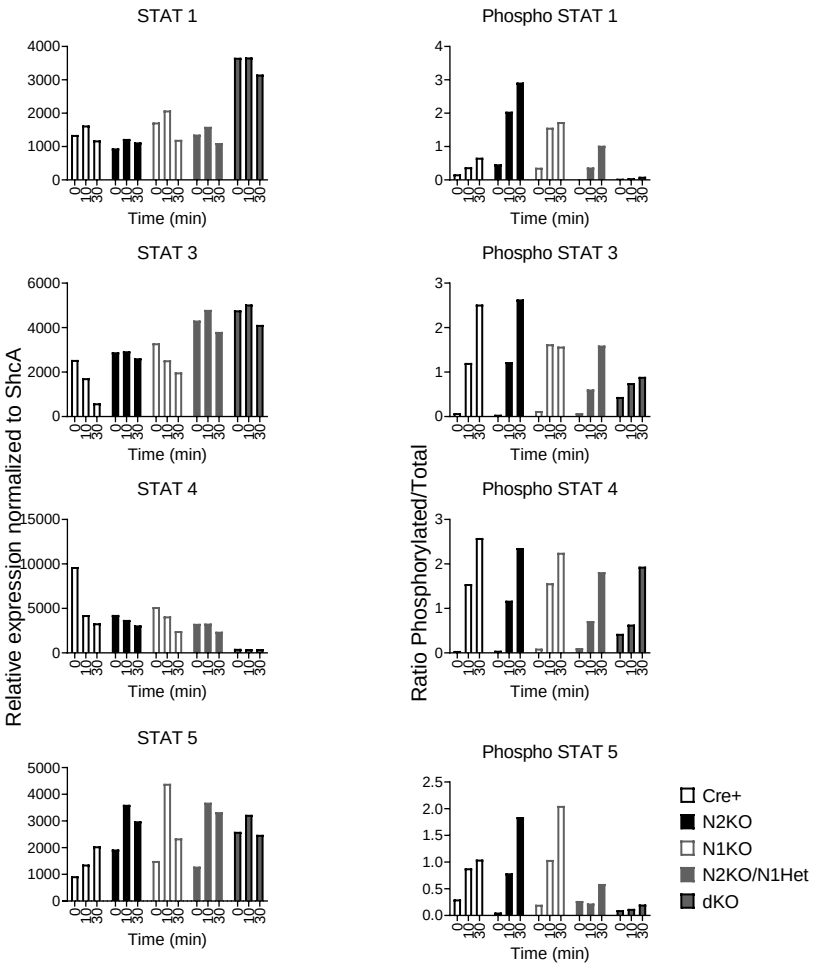
STAT 1
Phospho STAT 1
STAT 3
Phospho STAT 3
STAT 4
Phospho STAT 4
STAT 5
Phospho STAT 5
Relative expression normalized to ShcA
Ratio Phosphorylated/Total
Time (min)
Cre+
N2KO
N1KO
N2KO/N1Het
dKO

C

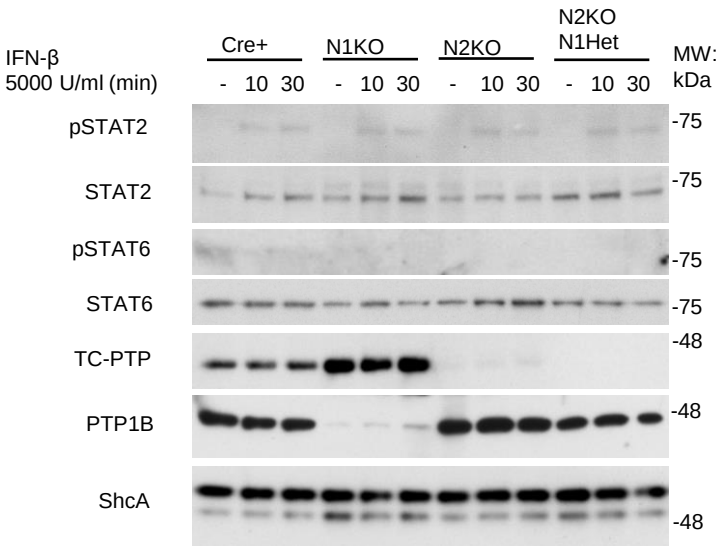
Cre+
N1KO
N2KO
N2KO N1Het
IFN-β 5000 U/ml (min)
- 10 30
MW: kDa
pSTAT2
STAT2
pSTAT6
STAT6
TC-PTP
PTP1B
ShcA
-75
-48

Figure 5

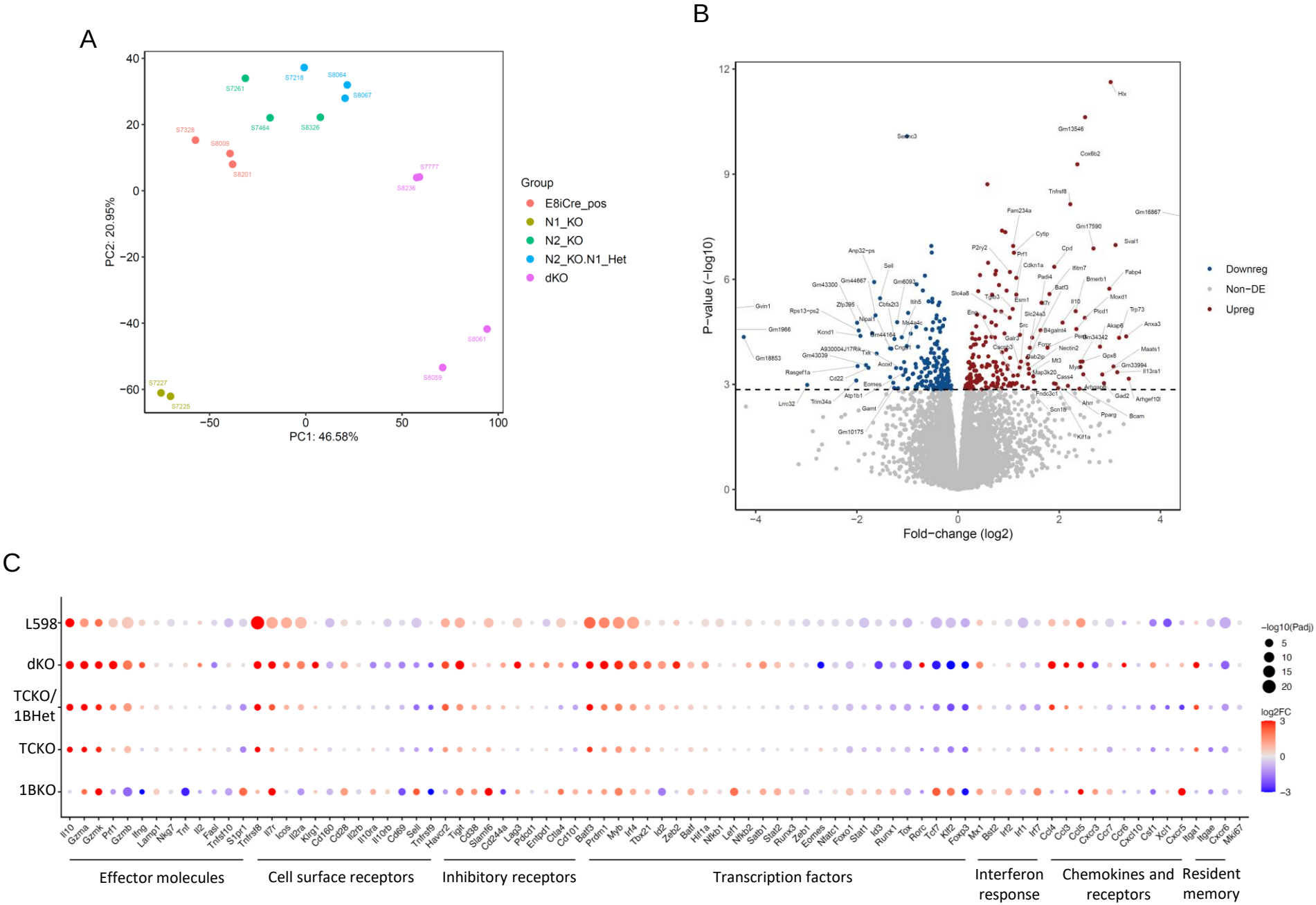
A
PC2: 20.95%
PC1: 46.58%
Group
E8iCre_pos
N1_KO
N2_KO
N2_KO.N1_Het
dKO
B
P−value (−log10)
Fold−change (log2)
Downreg
Non−DE
Upreg
C
L598
dKO
TCKO/ 1BHet
TCKO
1BKO
−log10(Padj)
log2FC
Effector molecules
Cell surface receptors
Inhibitory receptors
Transcription factors
Interferon response
Chemokines and receptors
Resident memory

Figure 6

A

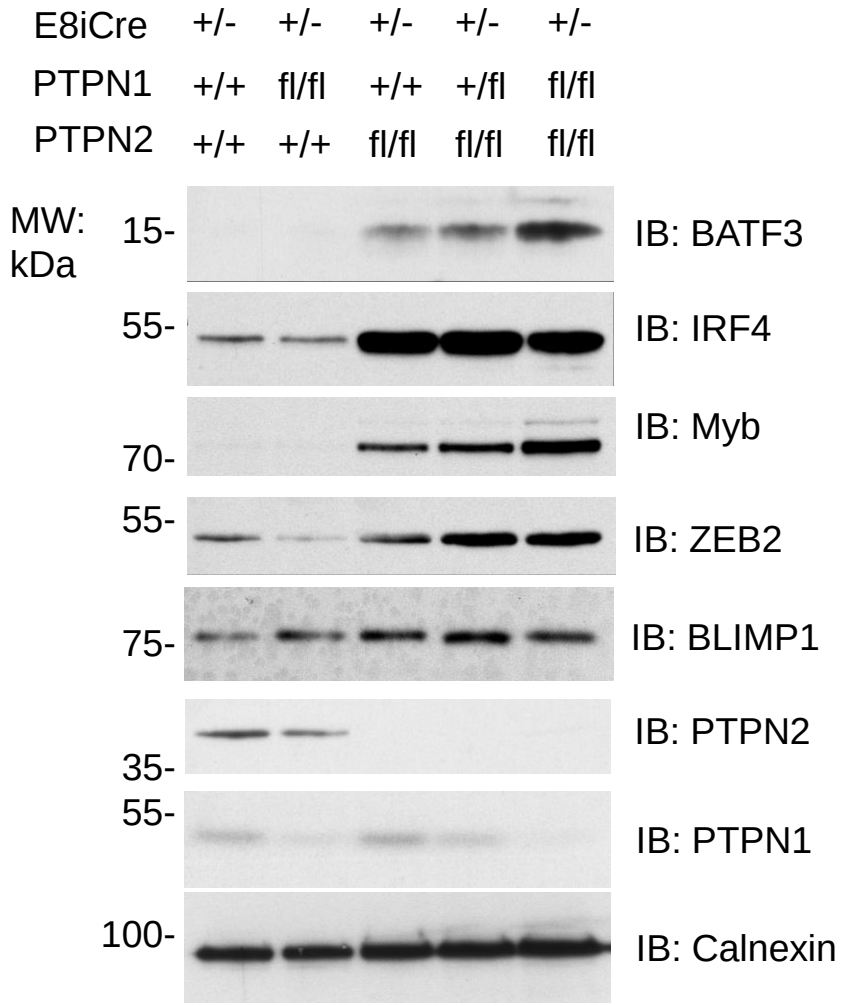
E8iCre +/- +/- +/- +/- +/-
PTPN1 +/+ fl/fl +/+ +/fl fl/fl
PTPN2 +/+ +/+ fl/fl fl/fl fl/fl
MW: kDa
15-
IB: BATF3
55-
IB: IRF4
70-
IB: Myb
55-
IB: ZEB2
75-
IB: BLIMP1
35-
IB: PTPN2
55-
IB: PTPN1
100-
IB: Calnexin

Figure 7

A

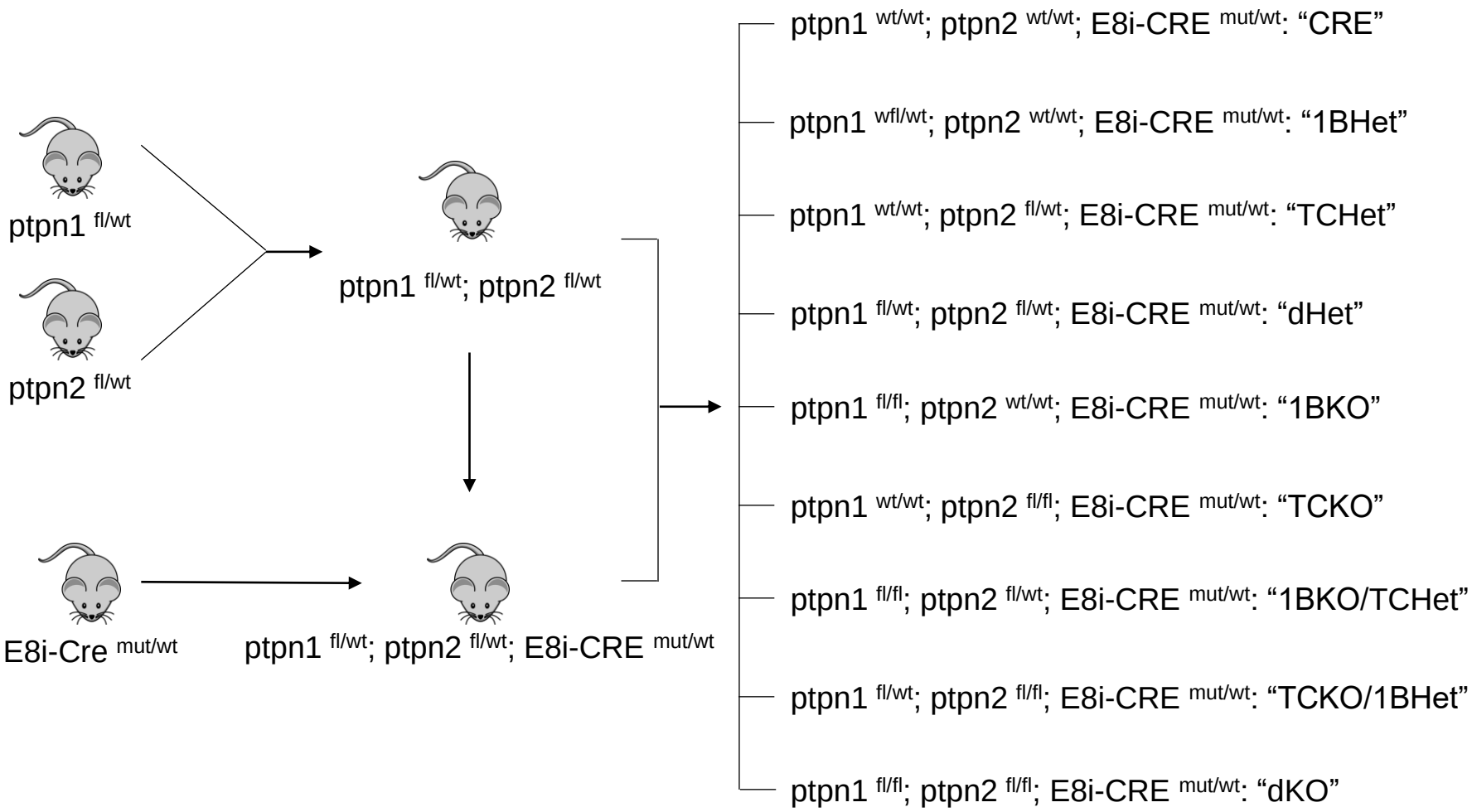

Figure S1

(Continue next page)

B

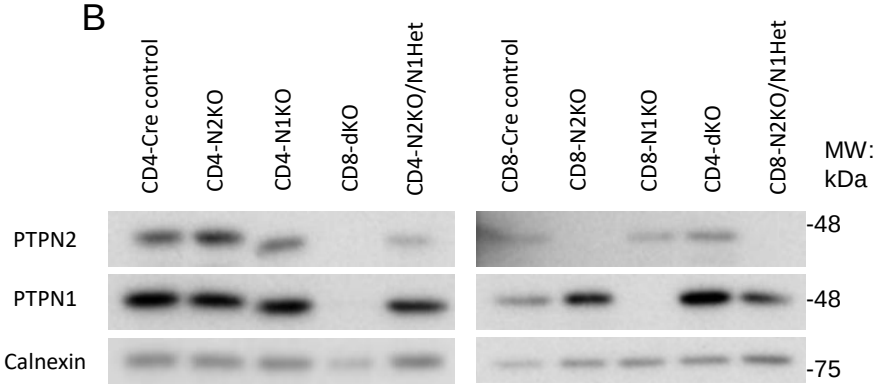

C

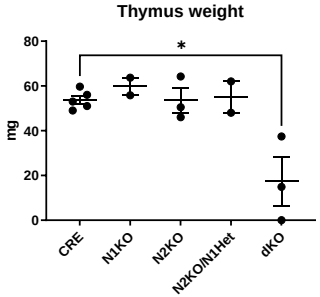

D

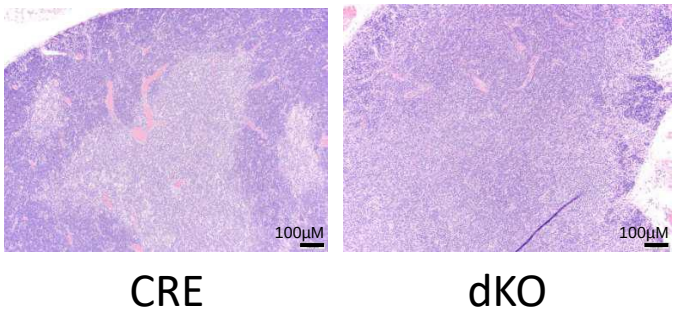

E

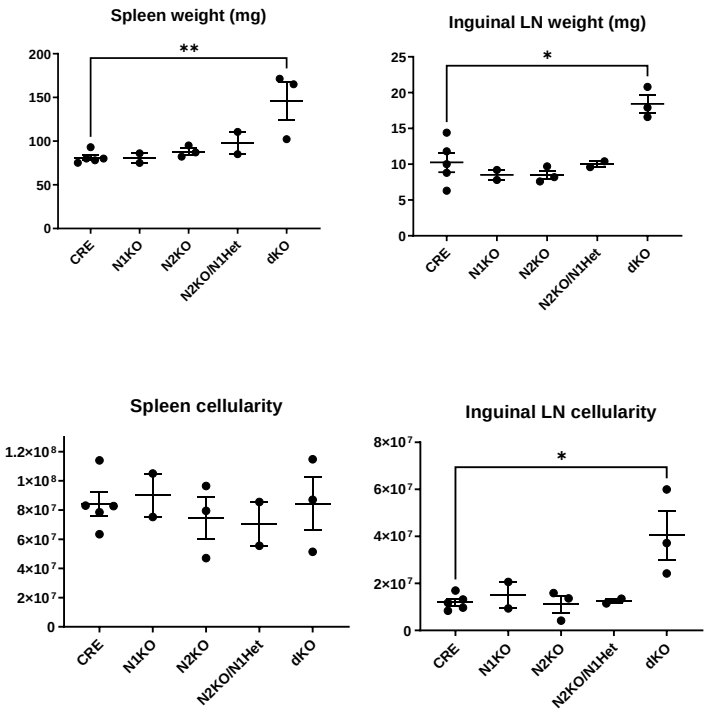

F

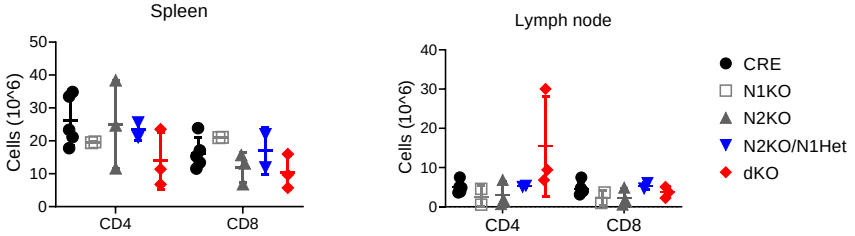

Figure S1

A

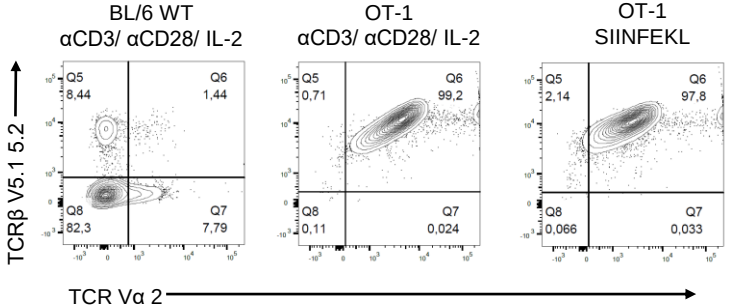

B

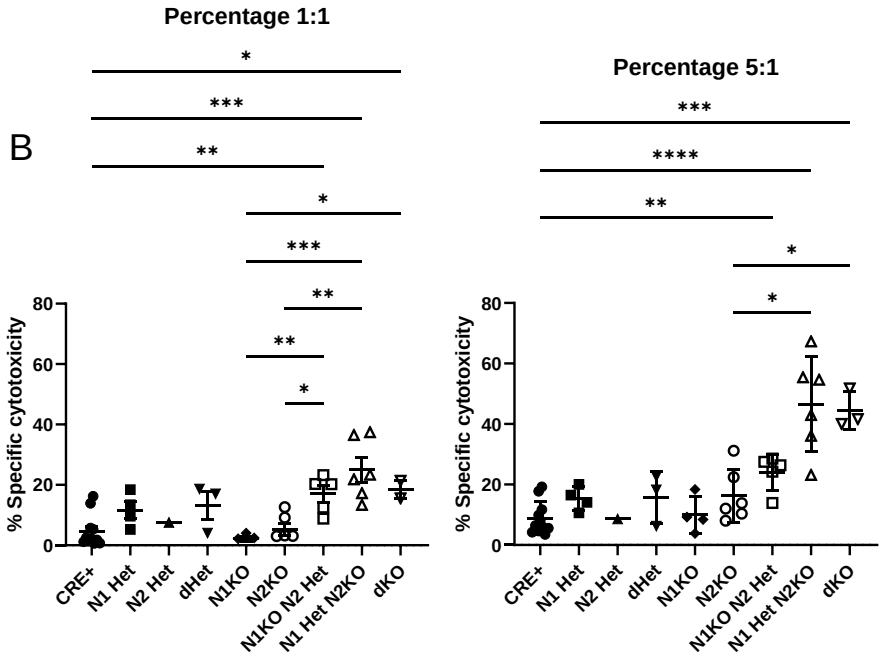

C

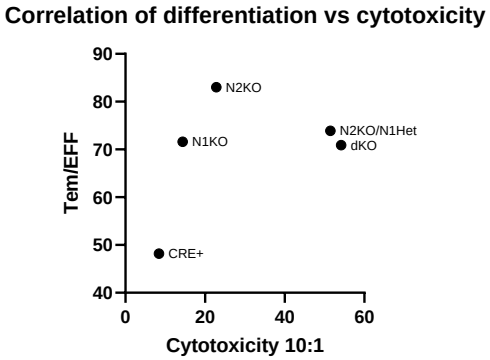

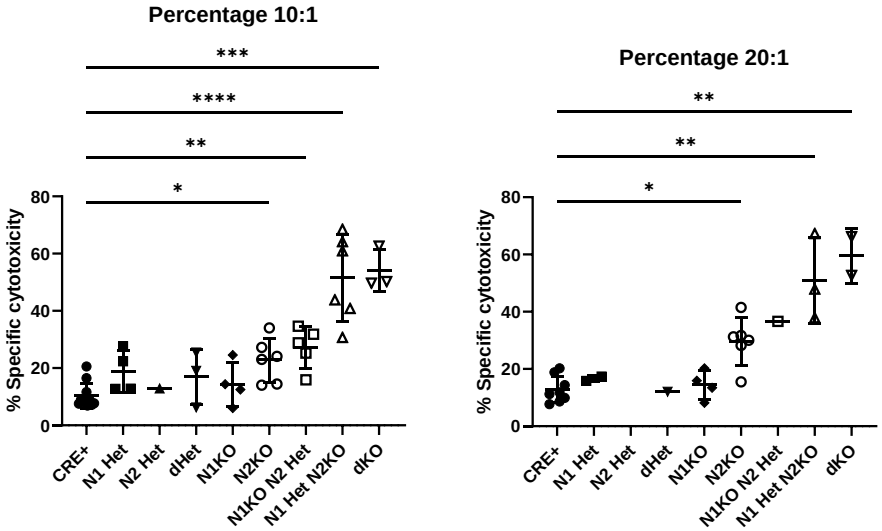

Figure S2

A

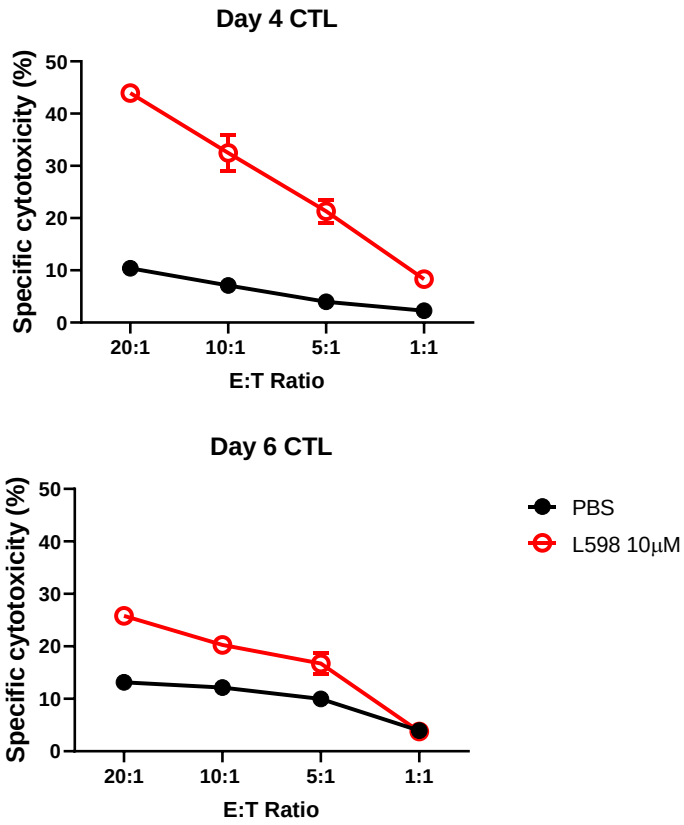
Day 4 CTL
Specific cytotoxicity (%)
50
40
30
20
10
0
20:1
10:1
5:1
1:1
E:T Ratio
Day 6 CTL
Specific cytotoxicity (%)
50
40
30
20
10
0
20:1
10:1
5:1
1:1
E:T Ratio
PBS
L598 10μM

B

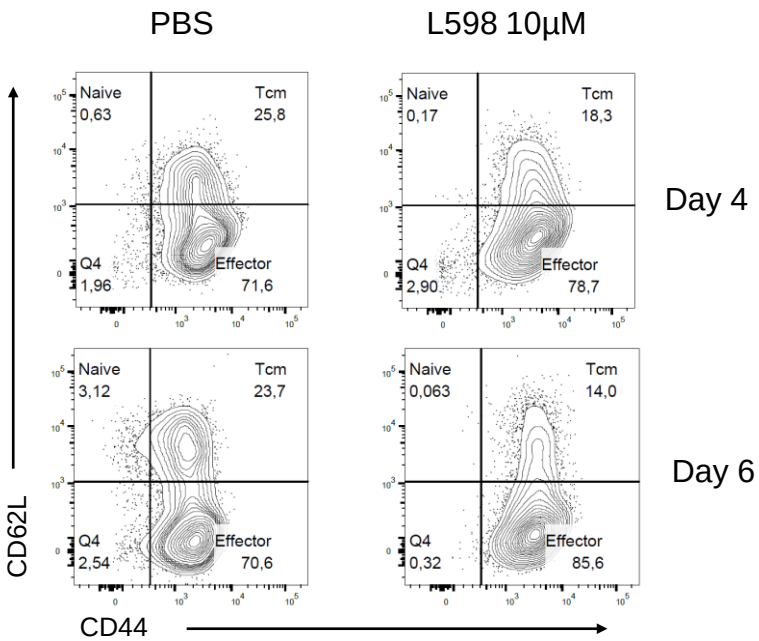
PBS
L598 10μM
Naive
0,63
Tcm
25,8
Q4
1,96
Effector
71,6
Naive
0,17
Tcm
18,3
Q4
2,90
Effector
78,7
Day 4
Naive
3,12
Tcm
23,7
Q4
2,54
Effector
70,6
Naive
0,063
Tcm
14,0
Q4
0,32
Effector
85,6
Day 6
CD62L
CD44

Figure S3

A

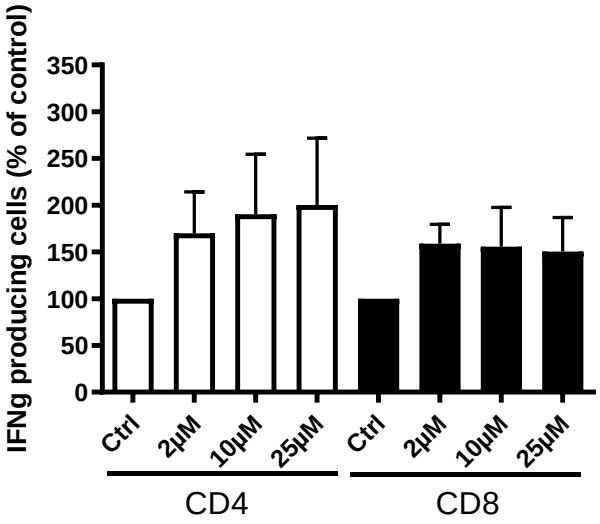

B

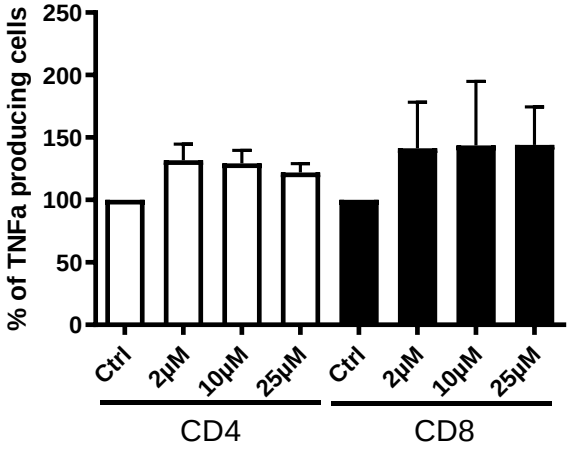

C

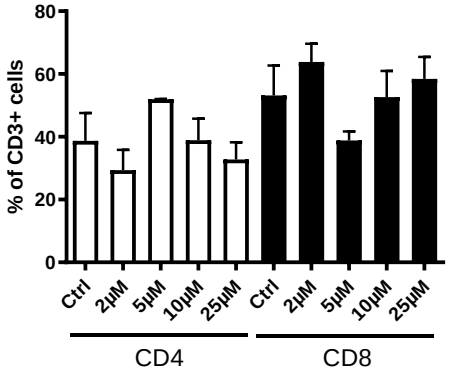

Figure S4

A

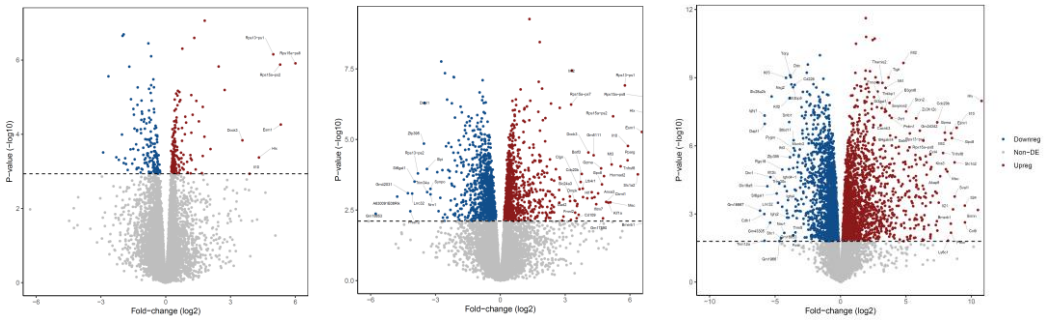

N2KO vs CRE

N2KO/N1Het vs CRE

dKO vs CRE

B

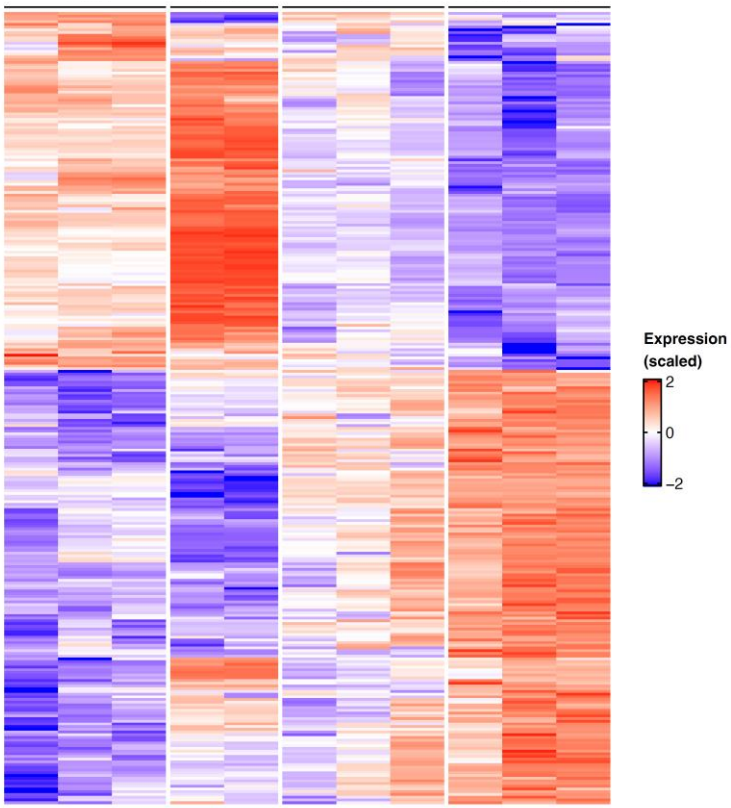

C

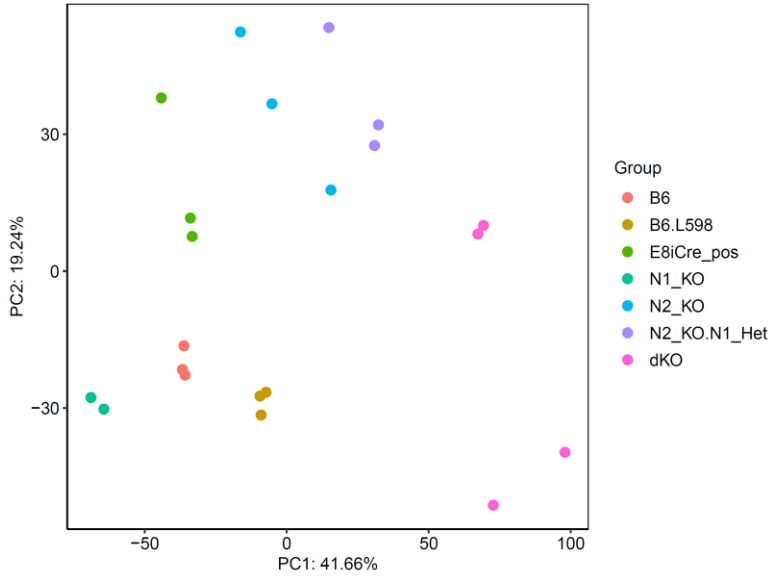

D

Gene	Nr4a1	Nr4a2	Nr4a3
N1_KO	-0.30663	-0.36716	-0.41666
N2_KO	-0.00153	-0.46813	0.386338
N2_KO.N1_Het	0.035497	-0.49453	-0.05114
dKO	2.029929	1.394544	0.526611
B6_vs_B6.L598	0.223162	-0.4296	0.366143

Figure S5

A

	N1KO	N2KO	N1 Het N2KO	dKO	L598
BATF3	2,50055	2,76642	3,8011	4,81526	2,27172
BLIMP-1	1,13592	1,789	2,4513	3,93185	2,10275
MYB	1,6224	1,52488	1,78499	2,84074	1,48583
IRF4	0,890283	0,97583	1,26343	2,49527	1,19417
ZEB2	0,081212	0,129684	0,935118	3,08974	1,01767
T-BET	0,506928	0,991337	0,913812	2,23344	0,246352
ID2	-1,00234	0,15541	0,752648	1,33523	0,191941
RUNX3	0,35036	0,228188	0,104463	0,424624	-0,2108
FOXO1	0,248335	-0,21162	-0,3079	-0,58246	-0,41948
EOMES	-0,41166	0,236346	-0,37881	-0,29639	-0,21736
ZEB1	-0,40898	-0,27215	-0,496	-0,17751	-0,66337
TCF7	1,75832	0,141233	-0,72336	-2,82384	-1,03225

Log2 of fold increase over Cre+ mice

Significant: FDR 5%

B

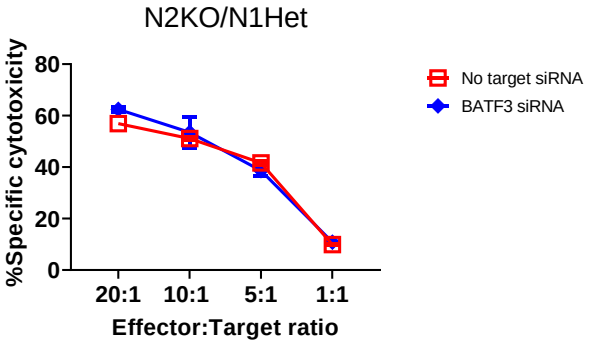

C

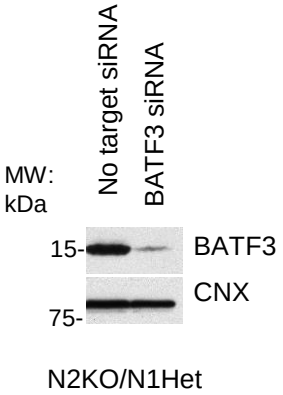

Figure S6